USGS
science for a changing world

Prepared in cooperation with the Nye County Nuclear Waste Repository Project Office

Characterization of the Highway 95 Fault in Lower Fortymile Wash using Electrical and Electromagnetic Methods, Nye County, Nevada

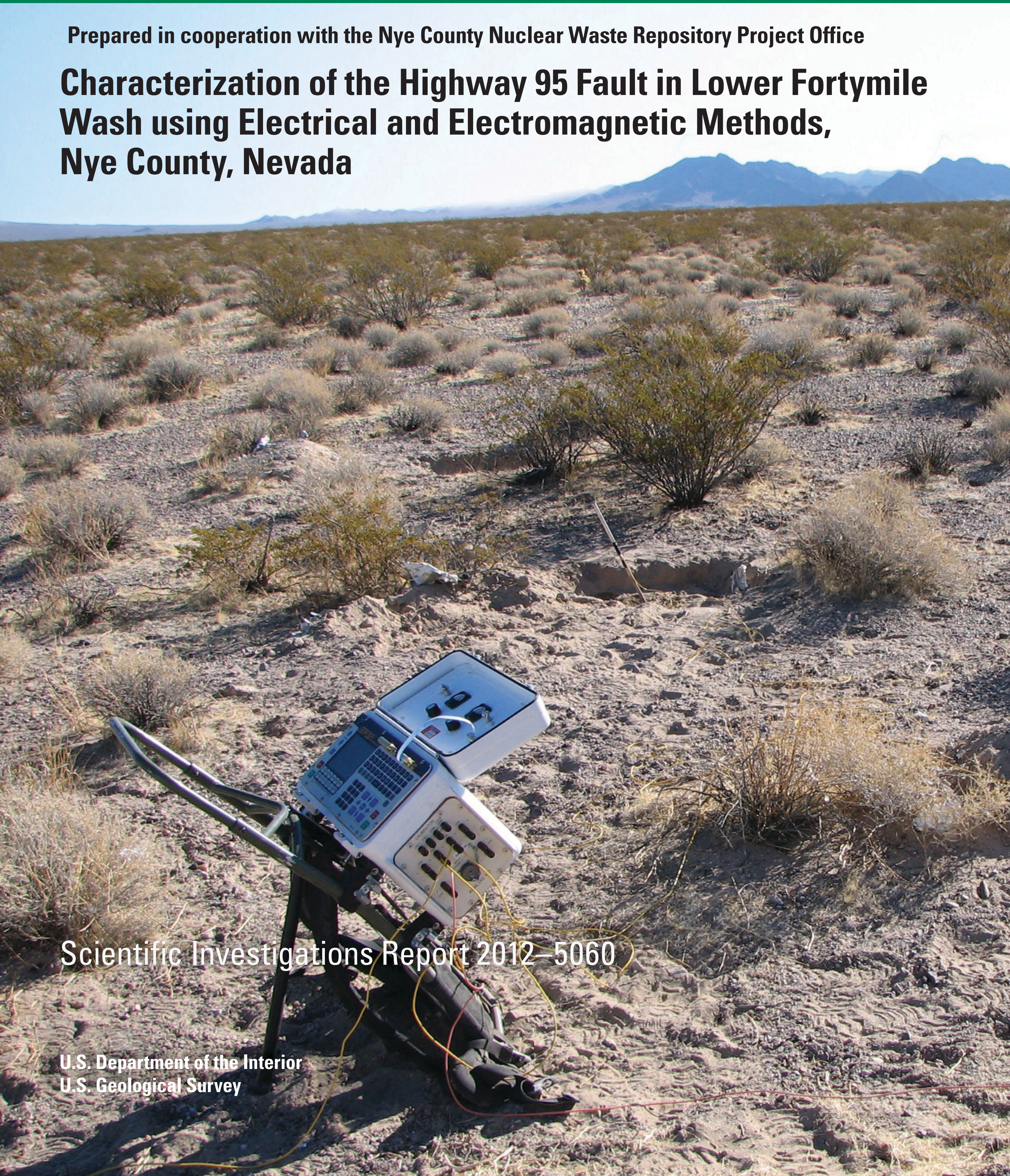

Scientific Investigations Report 2012–5060

U.S. Department of the Interior
U.S. Geological Survey

COVER
Photograph of a geophysical receiver in the Amargosa Desert, Nye County, Nevada (photograph by Jamie P. Macy).

Prepared in cooperation with the Nye County Nuclear Waste Repository Project Office

Characterization of the Highway 95 Fault in Lower Fortymile Wash using Electrical and Electromagnetic Methods, Nye County, Nevada

By Jamie P. Macy[1], Levi Kryder[2], and Jamieson Walker[2]

[1] U.S. Geological Survey

[2] Nye County Nuclear Waste Repository Project Office

Scientific Investigations Report 2012–5060

U.S. Department of the Interior
U.S. Geological Survey

U.S. Department of the Interior
KEN SALAZAR, Secretary

U.S. Geological Survey
Marcia K. McNutt, Director

U.S. Geological Survey, Reston, Virginia: 2012

This report and any updates to it are available online at:
http://pubs.usgs.gov/sir/2012/5060/

For more information on the USGS—the Federal source for science about the Earth,
its natural and living resources, natural hazards, and the environment,
visit http://www.usgs.gov or call 1-888-ASK-USGS (1-888-275-8747).

For an overview of USGS information products, including maps, imagery, and publications,
visit http://www.usgs.gov/pubprod

To order this and other USGS information products, visit http://store.usgs.gov

Suggested citation:
Macy, J.P., Kryder, Levi, and Walker, Jamieson, 2012, Characterization of the Highway 95 Fault in lower Fortymile Wash using electrical and electromagnetic methods, Nye County, Nevada: U.S. Geological Survey Scientific Investigation, Report 2012-5060, 44 p.

Contents

Figures

Conversion Factors

Inch/Pound to SI

Multiply	By	To obtain
	Length	
centimeter (cm)	0.3937	inch (in.)
meter (m)	3.281	foot (ft)
kilometer (km)	0.6214	mile (mi)
meter (m)	1.094	yard (yd)
	Area	
square meter (m^2)	0.0002471	acre
square kilometer (km^2)	0.3861	square mile (mi^2)
	Energy	
joule (J)	0.0000002	Kilowatt hour (kWh)
	Leakance	
meter per day per meter [(m/d)/m]	1	foot per day per foot [(ft/d)/ft]
millimeter per year per meter [(mm/yr)/m]	0.012	inch per year per foot [(in/yr)/ft]

Temperature in degrees Celsius (°C) may be converted to degrees Fahrenheit (°F) as follows:

°F=(1.8×°C)+32

Temperature in degrees Fahrenheit (°F) may be converted to degrees Celsius (°C) as follows:

°C=(°F-32)/1.8

Vertical coordinate information is referenced to the insert datum name (and abbreviation) here, for instance, “North American Vertical Datum of 1988 (NAVD 88)”

Horizontal coordinate information is referenced to the insert datum name (and abbreviation) here, for instance, “North American Datum of 1983 (NAD 83)”

Altitude, as used in this report, refers to distance above the vertical datum.

This page intentionally left blank.

Characterization of the Highway 95 Fault in Lower Fortymile Wash using Electrical and Electromagnetic Methods, Nye County, Nevada

By Jamie P. Macy, Levi Kryder, and Jamieson Walker

Abstract

The Highway 95 Fault is a buried, roughly east-west trending growth fault at the southern extent of Yucca Mountain and Southwestern Nevada Volcanic Field. Little is known about the role of this fault in the movement of groundwater from the Yucca Mountain area to downgradient groundwater users in Amargosa Valley. The U.S. Geological Survey (USGS) Arizona Water Science Center (AZWSC), in cooperation with the Nye County Nuclear Waste Repository Project Office (NWRPO), has used direct current (DC) resistivity, controlled-source audio magnetotelluric (CSAMT), and transient electromagnetics (TEM) to better understand the fault. These geophysical surveys were designed to look at structures buried beneath the alluvium, following a transect of wells for lithologic control. Results indicate that the fault is just north of U.S. Highway 95, between wells NC-EWDP-2DB and -19D, and south of Highway 95, east of well NC-EWDP-2DB. The Highway 95 Fault may inhibit shallow groundwater movement by uplifting deep Paleozoic carbonates, effectively reducing the overlying alluvial aquifer thickness and restricting the movement of water. Upward vertical hydraulic gradients in wells proximal to the fault indicate that upward movement is occurring from deeper, higher-pressure aquifers.

From December 2006 to January 2007, the USGS and NWRPO collected dipole-dipole DC resistivity data to characterize the Highway 95 Fault. Modeled data from the resistivity study agreed with mapped faults from gravity anomalies and highlighted a prominent fault within 1.5 km of Highway 95, thought to be the Highway 95 Fault. Results of the dipole-dipole resistivity survey warranted further study.

From March to April of 2008, the USGS and Nye County continued their geophysical investigation of the Highway 95 Fault using TEM and CSAMT geophysical techniques. TEM and CSAMT data were collected along the same profile as the dipole-dipole resistivity data. Modeled data from these additional studies yielded similar results to the dipole-dipole resistivity study. An area of distinct resistivity change was detected within 1.5 km of Highway 95, and it is thought that this change is the Highway 95 Fault.

Coordinated application of electrical and electromagnetic geophysical methods provided better characterization of the Highway 95 Fault. The comparison of dipole-dipole resistivity, TEM, and CSAMT data confirm faulting of an uplifted block of resistive Paleozoic Carbonate that lies beneath a more conductive sandstone unit. A more resistive alluvial basin-fill unit is found above the sandstone unit, and it constitutes only about 150 m of the uppermost subsurface.

Introduction

Yucca Mountain, Nevada, was designated by the Nuclear Waste Policy Act of 1982 (as amended) as the sole location for construction of a high-level nuclear-waste repository (fig. 1). Scientific data collection and characterization efforts by the U.S. Department of Energy (DOE), associated with development of the repository typically were limited to the area immediately surrounding the repository. In order to be able to predict groundwater travel times from Yucca Mountain south to the populated area of Amargosa Valley (fig. 1) accurately, additional data collection was required (fig. 2). Transport in groundwater is considered to be the primary mechanism by which radionuclides escaping the repository can reach the water table and be transported to the population in Amargosa Valley. Knowing the time required for groundwater to move from the repository to the Amargosa Valley is critical to protecting the health and welfare of downgradient water users. Nye County's Nuclear Waste Repository Project Office (NWRPO) drilled and completed a network of observation wells to help in determining the travel time of groundwater (fig. 3). Geophysical data collection was determined to be the most cost-effective method for obtaining additional complex subsurface geologic and hydrologic information. Geophysical data provide information about resistivity contrasts in the subsurface, which are useful for locating faults that are unidentifiable at the surface.

Purpose and Scope

This report presents the findings from a surface-geophysical investigation of the Highway 95 Fault in lower Fortymile

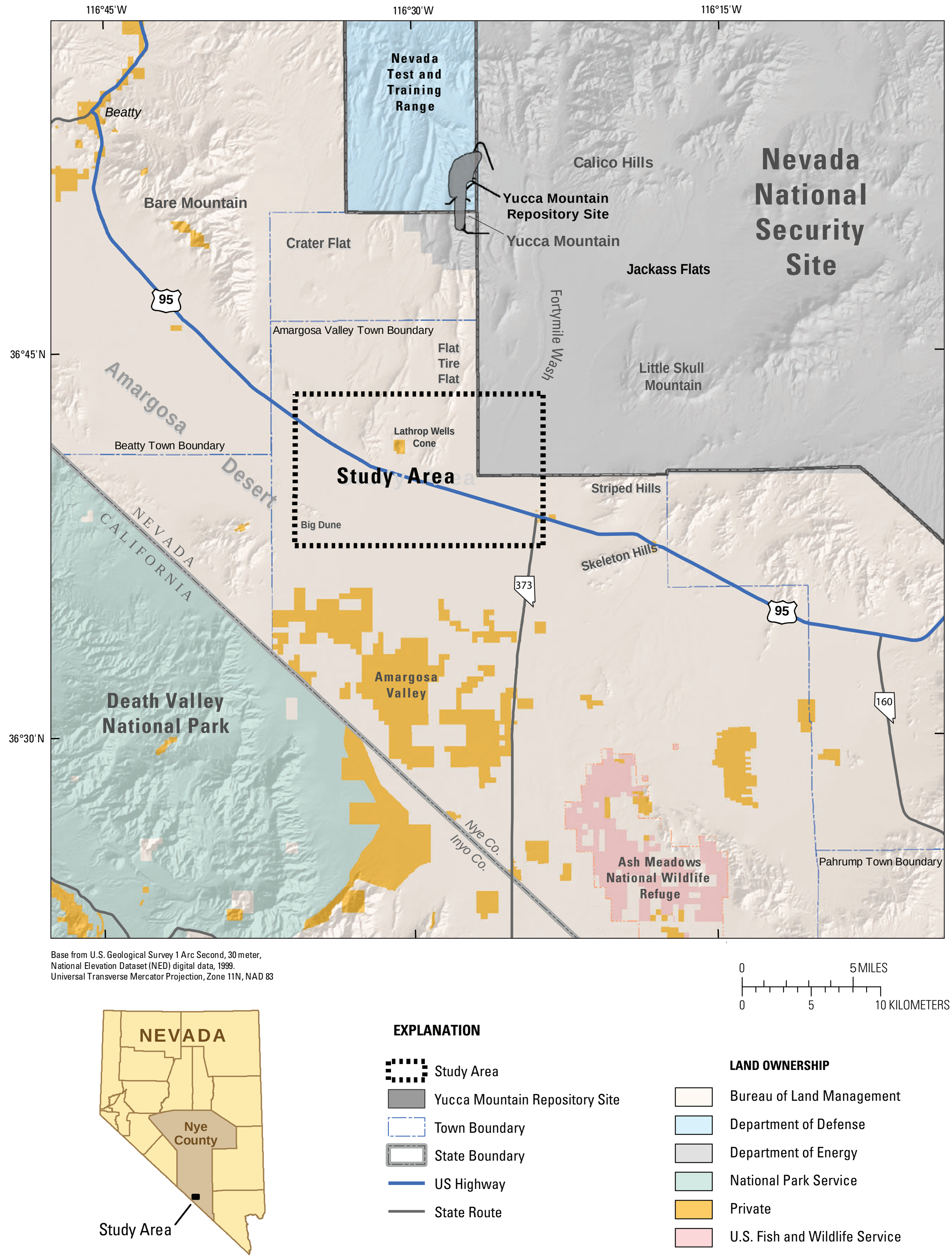

Figure 1. Map showing study area and surrounding regions in Nye County, Nevada, and Inyo County, California.

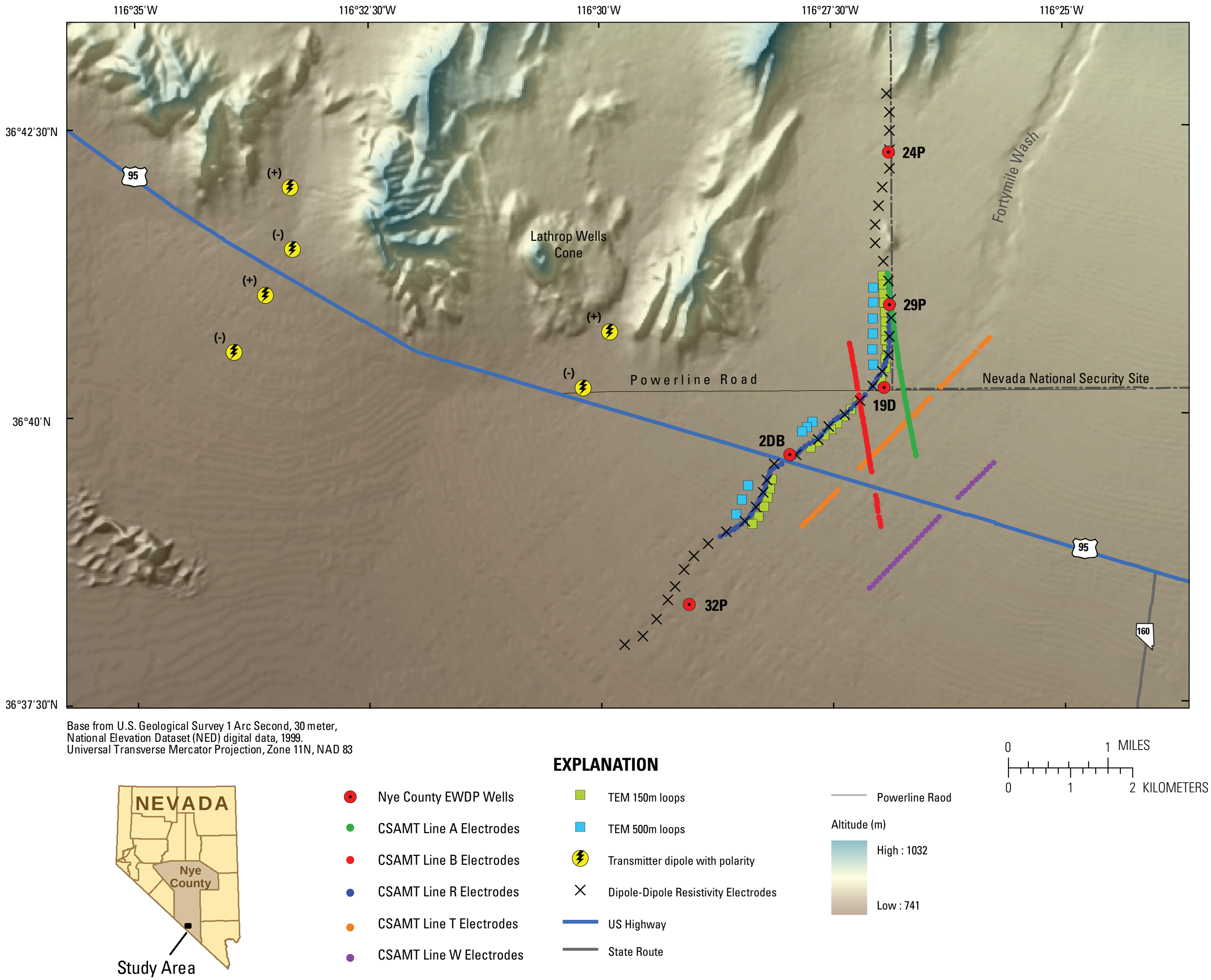

Figure 2. Map showing location of geophysical surveys and electrode placement in the study area, lower Fortymile Wash, Nye County, Nevada.

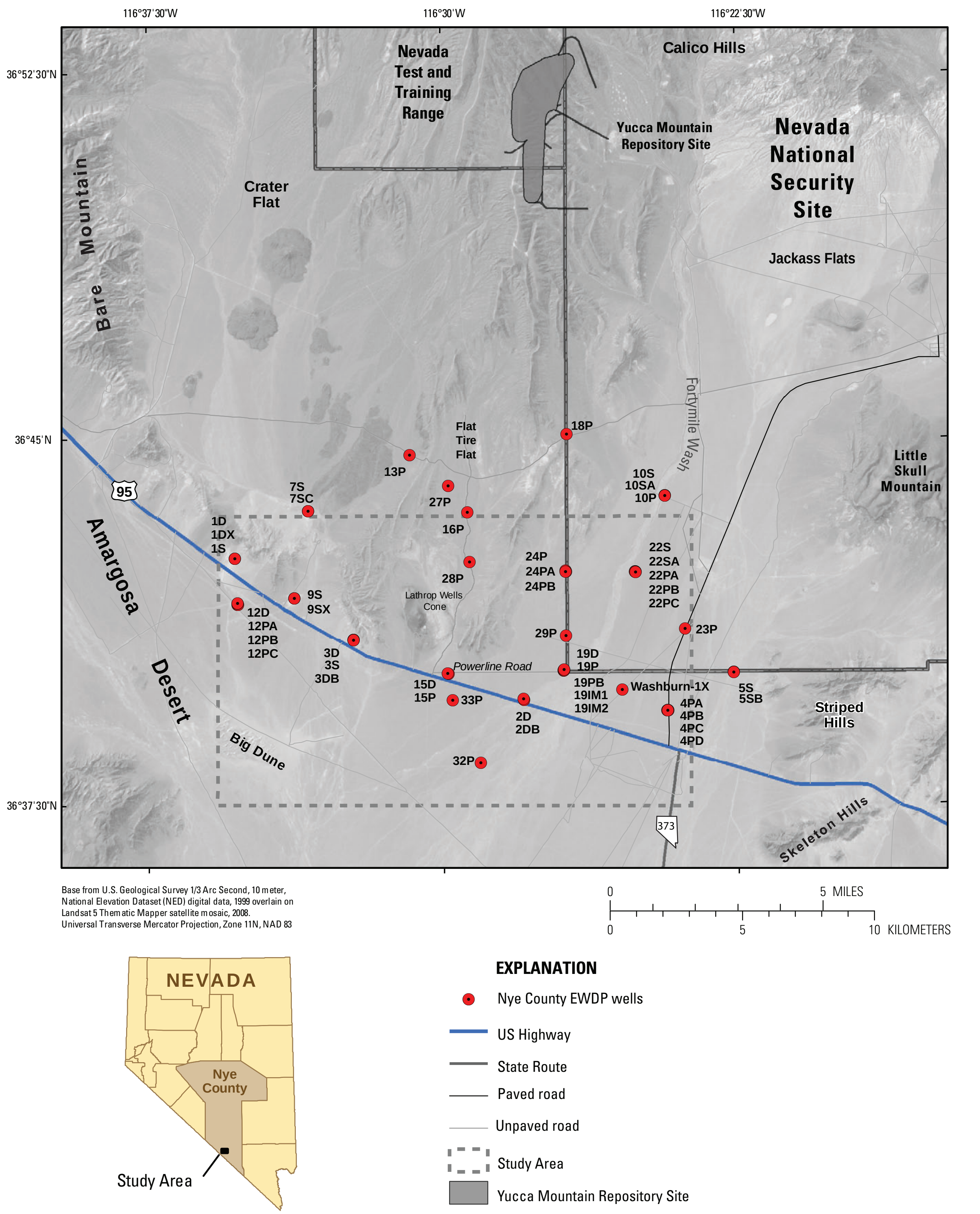

Figure 3. Observation well locations for the Nye County Early Warning Drilling Program (EWDP) (modified from Nuclear Waste Repository Project Office, 2009).

Wash, Nye County, Nevada. The report describes the hydrogeologic units near the Highway 95 Fault and the surface-geophysical techniques used for the investigation which includes dipole-dipole direct current (DC) resistivity, transient electromagnetics (TEM), and controlled source audio-frequency magnetotellurics (CSAMT). The theory, approach, raw data, data modeling, and results for each technique are described. Although associated water-level data and stratigraphic relations have been examined, the Highway 95 Fault System is complex and its hydraulic nature is not well-understood. The geophysical studies described in this report are intended to better characterize this complex fault system and to determine how it affects groundwater flows, both locally and regionally.

The work described in this report is a cooperative effort between the NWRPO and the USGS AZWSC.

Acknowledgments

Field work was done jointly by the USGS AZWSC and the NWRPO. The authors extend their appreciation to John Klenke of the Nye County NWRPO for his extensive effort as field crew chief throughout the geophysical surveys. Much appreciation also is extended to Craig Latronico, Ryan Lee, Bob Wilcoxon, and Judd Sampson from the Nye County NWRPO for their efforts and long hours spent assisting in data collection. The authors also would like to thank Jessica Gardner from the USGS AZWSC for her time and hard work during data acquisition.

Description of Study Area

Field work for these studies was done in southern Jackass Flats and northern Amargosa Desert, near lower Fortymile Wash (fig. 1). Lower Fortymile Wash is the major topographic drainage for Jackass Flats and the upland region of the southwest corner of the Nevada National Security Site. This area is bounded to the north by Calico Hills and Yucca Mountain, to the east by Little Skull Mountain, to the south by the town of Amargosa Valley, and to the west by Bare Mountain (fig. 1).

The topography is higher in the northern part of Jackass Flats, sloping gently to the south, however, large topographic variations exist locally where channels of Fortymile Wash are incised into the alluvial surface. This region of Nevada is arid, receiving approximately 4 inches of rain per year. Most of this precipitation occurs as rain during the winter months. Occasionally, runoff-inducing storms occur, and the washes flow. Such events are rare, and none occurred during the work detailed in this report.

Hydrogeology

Yucca Mountain is along the southern margins of the Miocene-age Southwest Nevada Volcanic Field (Fridrich, 1999; fig. 4). The mountain is a cuesta of thick, welded ash-flow tuff sheets bounded to the west by the Solitario Canyon-Windy Wash Fault System, a steeply dipping, north-northeast trending, down-to-the-west normal fault, and to the east by the similar Paintbrush Canyon and Bow Ridge Faults (fig. 4). The east-facing, gentle dip slope bedrock exposure is dominated by the resistant Tiva Canyon Tuff of the Paintbrush Group. The upper stratigraphy of the mountain consists primarily of welded outflow Miocene tuffs from calderas to the north, including the tuff member of the Claim Canyon caldera, principally the Topopah Spring Tuff and Tiva Canyon Tuff members of the Paintbrush Group, locally overlain by eroded remnants of the tuff members of the Timber Mountain caldera, principally the Rainier Mesa Tuff and Ammonia Tanks Tuff of the Timber Mountain Group (fig. 5). Underlying the Paintbrush Group tuffs, are the Crater Flat Group, a more regionally extensive volcanic group consisting of the Prow Pass Tuff, Bullfrog Tuff, and the Tram Tuff (fig. 4). These tuff members form the principle aquifer units beneath Yucca Mountain. Underlying the volcanic section are extensive “older” volcanic rocks and volcaniclastic sedimentary rocks comprising a fine-grained “muddy” sequence overlying the unconformity with lower Paleozoic rocks. Locally, above the unconformity, a basal sequence of fresh water limestones and coarse conglomerates is found (Fridrich, 1999; Potter and others, 2002; Nuclear Waste Repository Project Office, 2009; fig. 4).

Yucca Mountain forms an uplifted arcuate bedrock ridge between Jackass Flats to the east and Crater Flat to the west (fig. 4). Collectively, the area forms a large graben feature filled with Tertiary-age volcanic rocks between the east-dipping Bare Mountain Fault (west of Crater Flat) and the west-dipping “gravity fault” (east of Jackass Flats), defining the Crater Flat structural basin (Fridrich, 1999). The northern extent of the Crater Flat basin is bounded by the Yucca Wash Fault, a complex, buried, northwest-striking right-slip fault. The southern extent is bounded by the buried Highway 95 Fault (fig. 4), probably a reactivated Oligocene right-slip fault with subsequent dip-slip movement during the period of voluminous Miocene silicic eruptions that was buried by subsequent post-volcanic valley-fill sediments and younger alluvium in northern Amargosa Valley. The Highway 95 Fault forms the termination of the thick ashflow sheets of the Southwest Nevada Volcanic Field (fig. 4) and juxtaposes deep Paleozoic limestones against younger tuffaceous material (Fridrich, 1999; Nuclear Waste Repository Project Office, 2009). The offset Paleozoic carbonate unit may inhibit shallow groundwater movement, effectively reducing the overlying alluvial aquifer thickness and restricting the movement of water.

The upper volcanic-dominated groundwater-flow system of the Crater Flat structural basin is divided into two isolated north-south panels or domains, a western and an eastern domain, probably separated by structural offset along the Solitario Canyon/Windy Wash Fault System (Nuclear Waste Repository Project Office, 2009; fig. 4). The western domain, between the Bare Mountain Fault and Solitario Canyon/Windy Wash Fault System, has a southward-directed flow,

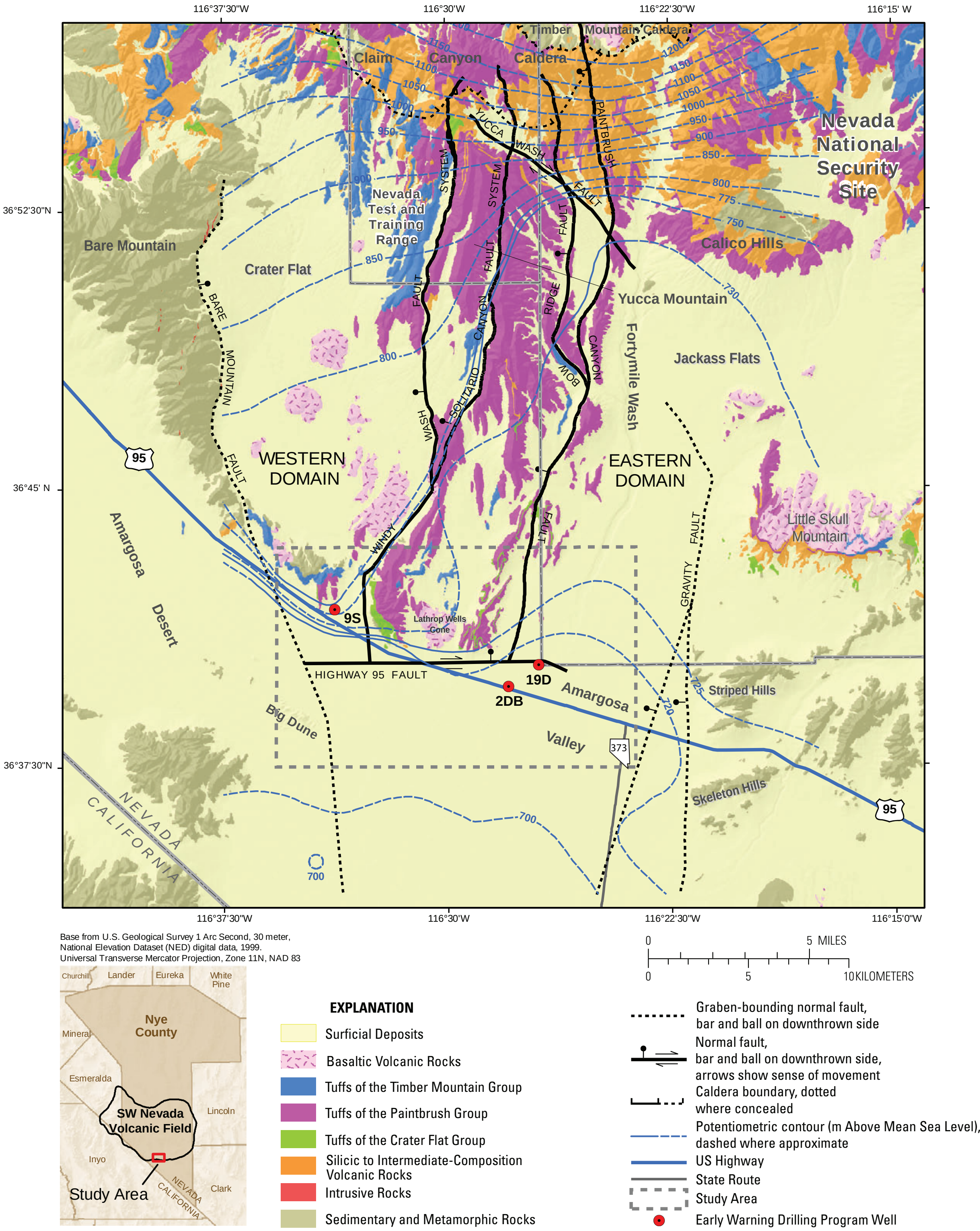

Figure 4. Map showing potential f ow barrier structures associated with the eastern and western groundwater f ow systems (from Potter and others, 2002). Surficial deposits and rock units (all ages) from Workman and others, 2002. Potentiometric contours adjusted from U.S. Department of Energy (2007) to include Early Warning Drilling Program EWDP Phase III and IV wells(Nuclear Waste Repository Project Office, 2009).

is hydraulically elevated, has a steep horizontal gradient, and discharges into Amargosa Valley near Nye County Early Warning Drilling Program (EWDP) well 9S (fig. 4). The eastern domain, between the Solitario Canyon/Windy Wash Fault System and the gravity fault, has a southeastward-directed flow, is hydraulically lower than the western domain, has a flat horizontal gradient, and discharges into Amargosa Valley along FortymileWash near Nye County EWDP wells 19D and 2DB (fig. 4).

Both the eastern and western domain groundwater-flow systems encounter the Highway 95 Fault at their southern extent where the volcanic hydrologic units terminate in northern Amargosa Valley (fig. 4). At the Highway 95 Fault, upward leakage from the underlying higher head carbonate aquifer mixes or displaces flow from the volcanic-dominated aquifer-flow system from the north at the transition to valley-fill-dominated flow in Amargosa Valley (Nuclear Waste Repository Project Office, 2009). This complex interplay of flow systems, hydraulic gradients, and structural-hydrologic connection along the Highway 95 Fault is difficult to model using the discrete subsurface drilling and well data available. Detailed geophysical survey information and interpretation, combined with the limited drilling and well information, will add to the understanding of this complex problem.

Previous Work by the Nye County Nuclear Waste Repository Project Office

The Nye County EWDP began in 1999, and its objective is to define the geologic units in the groundwater-flow system south of Yucca Mountain, between the repository and the town of Amargosa Valley, Nevada. Ultimately, this program supports the overall NWRPO mission to protect the health, safety, and economic well-being of the citizens of Nye County. The program is designed to provide prediction of the travel times of groundwater and associated contaminants related to radionuclides escaping Yucca Mountain and reaching the populated area of Amargosa Valley (fig. 1). The program is designed to collect geologic and hydrogeologic data directly through the drilling, installation, and testing of monitoring wells. To date, this phased program has produced 39 wells with 79 saturated-zone intervals in the southern Yucca Mountain, Fortymile Wash, Crater Flat, and northern Amargosa Desert areas (fig. 3). The resulting wells also are designed to serve as an early warning groundwater-monitoring network between the repository and present and future groundwater users in the Amargosa Valley.

Various data-collection programs overseen by the NWRPO for the EWDP, including aquifer and tracer tests, water-level monitoring, and water-sample collection and analysis, have produced a large amount of data. These data have been used by the DOE, Nye County, and others to define and refine aquifer characteristics, the groundwater-flow system, and contaminant transport mechanisms, to reduce uncertainty in groundwater models, to monitor trends in water levels over time, and to characterize the geochemical baseline and groundwater origin in the Yucca Mountain region.

Surface and borehole geophysical measurements made by the NWRPO have begun to characterize the hydraulic properties of the geologic units, the nature and continuity of alluvial layers, the areal distribution and variations in physical properties of the geologic units underlying the alluvium, and the hydraulic gradients within and between units.

Approach and Methodology

Three geophysical techniques were used for this study: dipole-dipole DC resistivity, TEM, and CSAMT. All three techniques involve measuring the resistivity of the Earth at depth by different electrical or electromagnetic techniques. Whereas dipole-dipole DC resistivity and CSAMT use electrical fields to calculate the resistivity of the Earth, TEM measures the Earth's resistivity by inducing magnetic fields. Resistivity is a measure of a material's opposition to the flow of electrical current and typically is measured in ohm-meters (ohm-m). Resistivity values for common near-surface earth materials vary by orders of magnitude, typically from 1,000 ohm-m or more for dry carbonates or crystalline rocks to 1 ohm-m or less for clays or alluvium saturated with high salinity water (Palacky, 1987). The resistivity of a rock is also dependent on saturation, porosity, fracturing, conductivity of fluids within the rock, and mineral composition (Zohdy and others, 1974). Saturated rocks have lower resistivities than unsaturated and dry rocks. Typical resistivities of sedimentary rocks, such as carbonates, can range from 100 ohm-m to 2,000 ohm-m, whereas shales or claystones can range from 1 ohm-m to 100 ohm-m, and sandstones can range from 20 ohm-m to 1,000 ohm-m. Igneous rocks, such as basalts, can range from 200 ohm-m to 1,000 ohm-m (Sumner, 1976; Nabighian and Macnae, 1987; Yungul, 1996). The higher the porosity of a rock, the lower the resistivity, and the higher the salinity of the saturating fluid, the lower the resistivity of the rock. The Earth's resistivity is calculated using Ohm's law:

$$V=IR \qquad (1)$$

where V is the measured potential across the receiver dipole in volts; I is the transmitted current across the transmitter dipole in amperes; and R is the resistance in ohms (Sumner, 1976). Electrical resistivity (ρ_a) depends on the distance and area across which the current is flowing, such that:

$$\rho_a = RA/L$$

where A is area and L is length (Telford and others, 1976).

This project began with a dipole-dipole DC resistivity survey following a transect of EWDP wells in the lower Fortymile

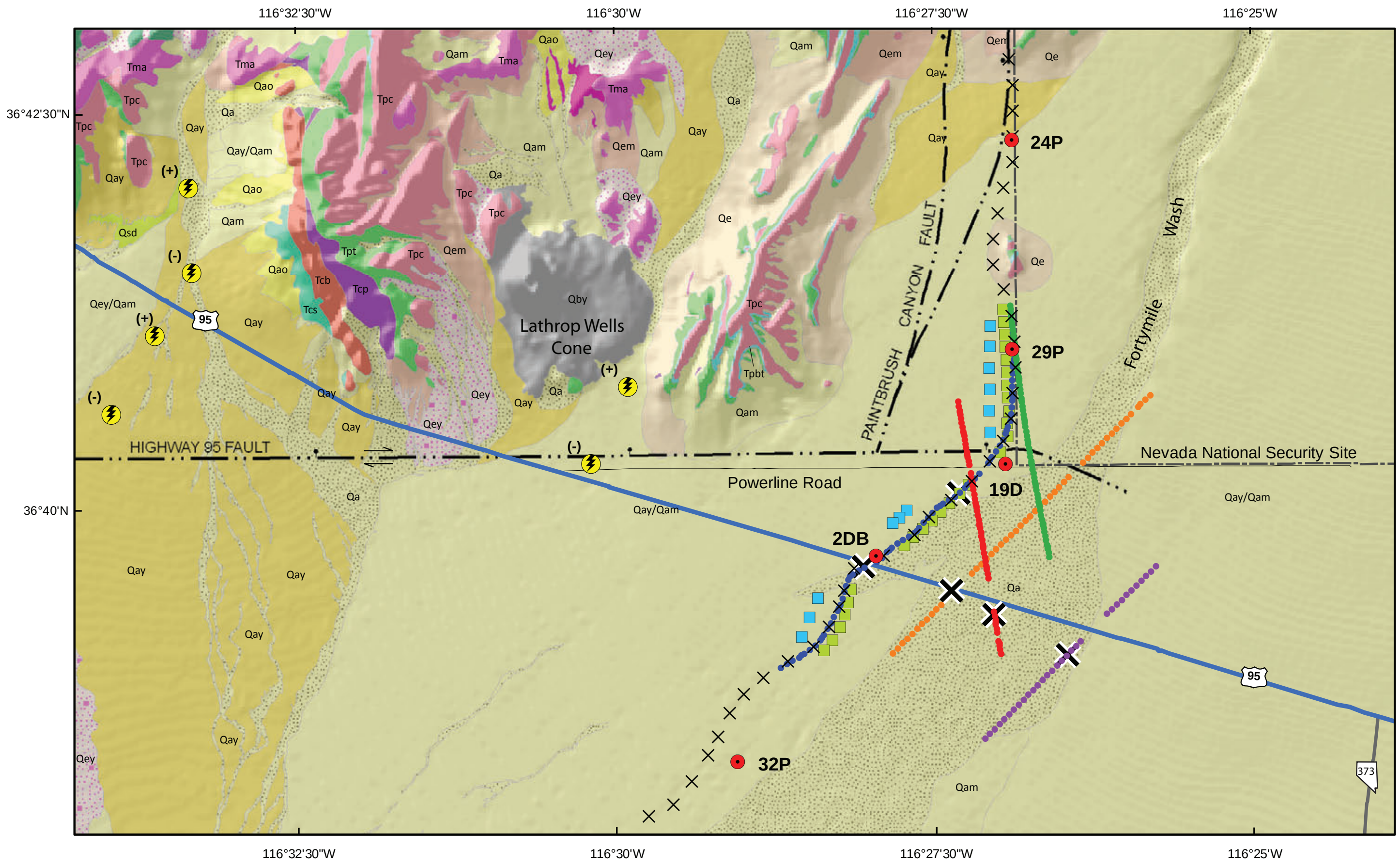

Base from U.S. Geological Survey 1 Arc Second, 30 meter,
National Elevation Dataset (NED) digital data, 1999.
Universal Transverse Mercator Projection, Zone 11N, NAD 83

0 1 MILES
0 1 2 KILOMETERS

EXPLANATION

- Nye County EWDP wells
- CSAMT Line A Electrodes
- CSAMT Line B Electrodes
- CSAMT Line R Electrodes
- CSAMT Line T Electrodes
- CSAMT Line W Electrodes
- TEM 150m loops
- TEM 500m loops
- Dipole-Dipole DC Resistivity Electrodes
- Transmitter bi-pole with polarity

GEOLOGIC UNITS

Qa	*Alluvium (Holocene)*
Qay	*Younger alluvium (Holocene and late Pleistocene)*
Qam	*Alluvium (late and middle Pleistocene)*
Qay/Qam	*mantle of Qay over Qam*
Qey/Qam	*mantle of Qey over Qam*
Qao	*Older alluvium (middle and early Pleistocene)*
Qey	*Eolian sand and fragments (Holocene and late Pleistocene)*
Qem	*Eolian-colluvial ramp deposits (Holocene to middle Pleistocene)*
Qe	*Eolian deposits (Holocene to middle Pleistocene)*
Qsd	*Spring deposits (Holocene to middle Pleistocene)*
Qby	*Younger Quaternary basalt (late Pleistocene)*

Timber Mountain Group (Miocene)

Tma	*Ammonia Tanks Tuff*
Tmr	*Rainier Mesa Tuff*

Paintbrush Group (Miocene)

Tpc	*Tiva Canyon Tuff*
Tpbt	*Bedded tuff (Paintbrush Gp.)*
Tpt	*Topopah Spring Tuff*

Crater Flat Group (Miocene)

Tcp	*Prow Pass Tuff*
Tcb	*Bullfrog Tuff*
Tcs	*Pre-Bullfrog Tuff bedded tuff*

- Interpreted Highway 95 Fault location
- Fault, Inferred, bar and ball on downthrown side, arrows show sense of movement

Figure 5. Geologic map of study area (modified after Potter and others, 2002) and locations of geophysical survey lines, Nye County, Nevada.

Wash. The resistivity survey follows an approximate north-to-south trending transect with a slight bend to the southwest about midway along the line. Additional geophysical data were collected along the same transect by using TEM and CSAMT techniques (fig. 5). TEM soundings were done only along the same transect as the resistivity profile. Additional CSAMT surveys were done throughout the lower Fortymile Wash area. During the studies described in this report, the geophysical lines generally were run over the desert surface, avoiding wash channels and other topographic features, such as hills, where possible. However, the south end of CSAMT Line T entered a gravel pit.

Data collected by using all three techniques were reduced to apparent resistivity values. Apparent resistivity is that which an instrument measures over a heterogeneous earth. It is a bulk average that is dependent upon many factors, including the particular electrical method being used (transient, frequency domain, direct-current injection) and instrument geometry, as well as spatial distribution and type of rocks, minerals, and solutes included in the sample volume. Because this complexity does not conform to simple models of averaging, and because the earth rarely has homogeneous and isotropic properties, an inverse model is developed to help constrain the distribution of electrical resistivities in the subsurface. Typically, inversion routines begin with forward models composed of layered rectangular blocks within individual resistivity values. The inverse model determines the calculated system response over the model area. Through iterations, the inversion process attempts to alter the model until the difference between the calculated and measured apparent resistivity values is minimized. The final model represents a non-unique estimate of the probable distribution of resistivity values in the subsurface. Each model presents the possible solutions for a given set of measurements, but only after the model is compared to other data can a true model be presented. Four 2-dimensional (2-D) inverse modeling software packages were used: (1) Loke RES2D for the dipole-dipole DC resistivity technique (Geotomo, Penang, Malaysia), (2) EMIGMA (PetRosEiKon, Toronto, Canada) and (3) STEMINV (Zonge Engineering, Tucson, Arizona) for the TEM technique, and (4) SCS2D (Zonge Engineering, Tucson, Arizona) for the CSAMT technique. The 2-D resistivity sections were then examined for distinct changes in resistivity, and interpretations were made based on the subsurface hydrogeologic system.

Dipole-Dipole Direct Current (DC) Resistivity

Dipole-dipole DC resistivity is a commonly used electrical technique for investigating the subsurface of the Earth. The advantage of dipole-dipole resistivity over other common resistivity techniques is the short potential and current dipoles necessary for exploring large depths (Zohdy and others, 1974). A Zonge resistivity acquisition system, which includes a Zonge GGT-30 transmitter and Zonge GDP-32 receiver, was used for this survey. A Zonge ETS-9 switch box was used to switch transmitting pairs of electrodes. For this technique, an electrical current is transmitted into the ground, and the resulting potential differences are measured at the surface (Sharma, 1997). Layers within the Earth that are electrically conductive or resistive will deflect or distort the normal potentials. Lateral resolution and depth of investigation are controlled by the dipole length. Four electrodes are used for a resistivity measurement, two transmitting (current, I) electrodes and two receiver (potential, V) electrodes (fig. 6). The spatial configuration of dipoles can be arranged in different ways to optimize the detection of subsurface electrical-structure geometries. Dipole-dipole resistivity surveys are configured with the potential electrodes outside of the current electrodes, with each pair having a constant mutual separation (Hallof, 1992). A separate dipole is created by each pair of electrodes (current or potential). In the typical dipole-dipole array, the distance between the pairs (na) is larger than the spacing of the dipole (a), as shown in figure 6 (Sharma, 1997). The equation for calculating dipole-dipole resistivity is:

$$\rho_a = (\pi) na(n+1)(n+2)V/I \qquad (2)$$

where ρ_a is the calculated apparent resistivity, n is the spacing between dipoles, a is the length of the dipole, V is the voltage, and I is the current.

Data collection for the dipole-dipole DC resistivity survey consisted of measurements made from November 13 to 17, 2006, December 11 to 15, 2006, and January 8 to 11 and 22 to 25, 2007. The survey line trended north to south with a bend to the southwest on the lower half of the survey (fig. 5). The electrodes in each dipole were 600 m apart. After each measurement the dipoles were moved 300 m to the next measurement location along the survey transect. The survey line was 10 km long, and large spacings between dipoles were necessary to achieve the desired depth of investigation.

The high contact resistance of the dry, coarse, sandy basin fill of the Amargosa Desert made it difficult to inject electricity into the ground. Traditionally, metal stakes are used for current and potential electrodes, but for this study, electrodes for transmitting the current consisted of aluminum-foil-lined pits that were excavated in the ground, and 24-inch metal stakes were used to measure the potential. The contact resistance at the surface was high, and the aluminum-foil-lined pits were necessary for the generator-powered transmitter to get enough current into the ground. Each current electrode consisted of between 3 and 6 pits, of which each pit was about 2 ft by 3 ft and dug to about 1 ft in depth. The pits were filled with salt water, lined with aluminum foil, backfilled, and watered again.

Repeat measurements were made at each potential dipole, and those measurements were averaged in Microsoft Excel and modeled using AGI Loke Res2D software (Geotomo Software, Penang, Malaysia).

Transient Electromagnetics (TEM)

A TEM sounding is made by transmitting an intermittent electrical signal through an ungrounded wire that is laid in a square loop on the surface of the earth (fig. 7). The transmitter loop (Tx) is energized periodically at regular intervals at frequencies of 4 to 32 hertz, and creates a time-varying magnetic field in the earth below it through Ampere's law (Fitterman and Stewart, 1986). According to Faraday's Law of Induction (Fitterman and Stewart, 1986), rapidly switching the electric signal on and off produces a primary electromagnetic field that diffuses into the ground and causes (induces) eddy currents in the ground and in nearby buried conductors (Sharma, 1997). The eddy currents create secondary magnetic fields some portion of which travel back to the surface (Nabighian and Macnae, 1987; fig. 7) where they can be measured as a decaying magnetic field. This usually is done by using a receiver composed of a smaller secondary loop or a vertical coil of highly conductive material. Although the secondary magnetic field can be measured anytime, many instruments focus on detecting the fields after the instrument stops transmitting. This gives the instrument greater sensitivity than other electrical methods because the decay of these currents occurs when there is no primary field to interfere with detection (Nabighian and Macnae, 1987).

Measurements of the decaying secondary field are made at the land surface by sampling the field during multiple short time windows. Measurements that are made with the receiver coil inside of the transmitter loop provide a 1-dimensional (1-D) estimation of the subsurface resistivity. Measurements made with the receiver coil outside of the transmitter loop can identify 2- or 3-dimensional variations in the subsurface that violate the boundary conditions of the inherently 1-D TEM soundings. Outside loop measurements are taken as far outside the loop as the desired depth of investigation. If the depth of investigation is 150 m, then a measurement outside the loop is made 150 m from the edge of the loop. Outside loop measurements can be made in any direction from the center, but for this study, outside loop measurements were made in opposing cardinal directions. For example, outside measurements at a single loop would be made at 150 m to the north of the loop and 150 m south of the loop.

The depth of investigation of a TEM sounding is dependent on the size of the primary loop, the amount of current excited into the loop, and the ability of the subsurface to conduct an electric field. A general rule of thumb is that the depth of investigation is about 2 to 3 times the size of the transmitter loop of wire. In conductive areas, the depth of investigation may only be equivalent to the size of the loop; and in more resistive areas, the depth of investigation may be more than 3

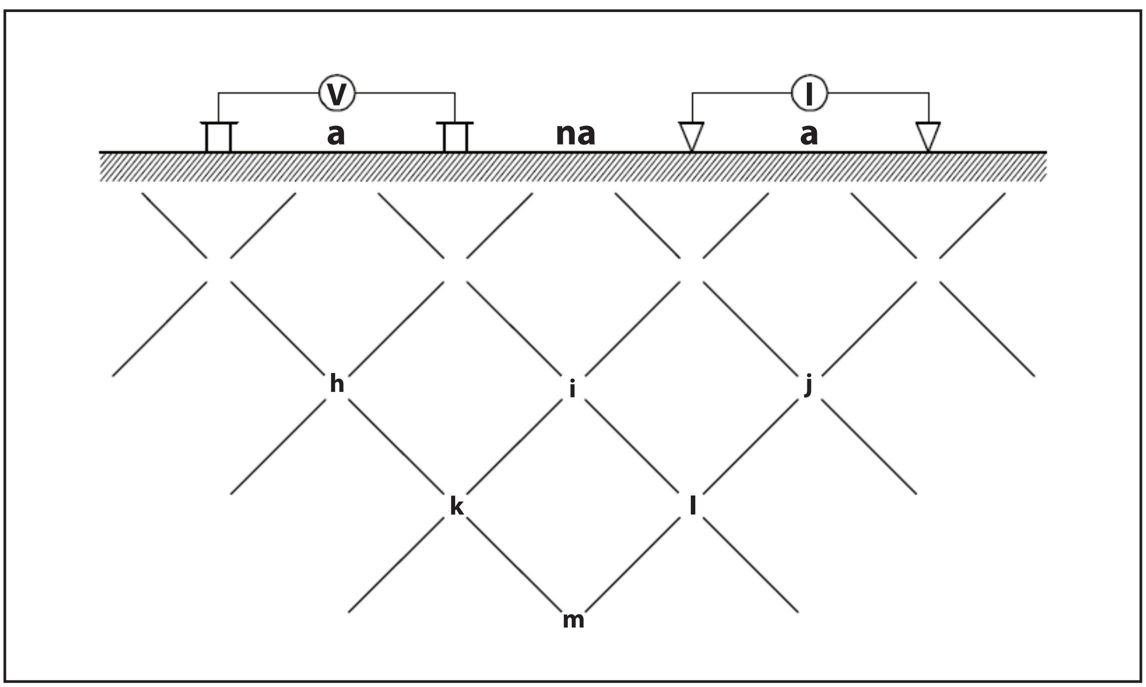

Figure 6. Diagram of dipole-dipole direct-current resistivity array. The dipoles are represented as **a**, and **na** is the relative spacing between current and potential electrodes. Electrical current is driven into the ground at the dipole marked **V**, and electrical potential is measured at dipole **I**. Points **h, i, j, k, l,** and **m** represent measured data points (after Hallof, 1992).

times the size of the primary loop (Zonge, 1992). Each TEM sounding is comparable to a single drilled borehole, although the sample volume is significantly larger because of the size of the transmitter loop and the outward spreading of the primary field with depth (smoke-ring effect). The results of an individual TEM sounding normally are plotted as resistivity values with depth. Multiple TEM soundings adjacent to or near each other can be plotted together as a TEM profile or cross section.

A Zonge Engineering ZeroTEM system (Zonge Engineering, Tucson, Arizona) was used for this investigation. The system was set up in 2 different loop-size configurations. The first configuration consisted of a Zonge ZT-20 transmitter connected to a 150 m by 150 m transmitter loop (Tx) that was excited with between 3.0 and 3.5 amps for each sounding. The second configuration was designed for deeper investigation, and it included a Zonge GGT-30 transmitter connected to a 500 m by 500 m Tx loop that was excited with 15 amps for each sounding. A Zonge TEM/3 antenna which has a 10,000 square-m moment was used in conjunction with a Zonge GDP-32II multifunction receiver (Rx) for all surveys. Multiple transmitter frequencies, 1, 2, 4, 8, or 16 hertz, were collected at each site with each configuration to obtain the deepest penetrating frequency with the least amount of noise at the end of the transient decay curve. Lower frequencies can allow for longer times when the instrument is not transmitting and, therefore, provide more time to detect secondary fields originating at greater depths. Frequencies commonly are chosen to obtain data from the greatest depth while minimizing noise. Depending on the frequency, twenty to twenty-five time windows of data were collected at each sounding from 0.0 μsec to 12.14 msec. Measured data were observed in the field as an averaged normalized return for each time window that were then graphed for visual inspection of irregularities. Three repetitions of each sounding were measured and averaged together.

TEM data can be influenced negatively by nearby metal conductors, such as fences, pipes, underground wires, overhead or buried power lines, and train tracks. Cultural interferences such as these were noted in lower Fortymile Wash and avoided when possible. One guideline for TEM soundings is to keep the sides of the Tx loop about 1 loop length away from any cultural interference. Loops for this study had 150 m sides for the first configuration and 500 m sides for the second configuration. Therefore, all cultural interference was kept at least 150 m from any side of the Tx loop for the first configuration, and cultural interference was kept 500 m from any side for the second configuration.

Raw TEM data were collected and then processed, and 1-D layered earth resistivity models were developed using Zonge Engineering's DATPRO suite of software. Raw TEM data were averaged using Zonge's TEMAVG program.

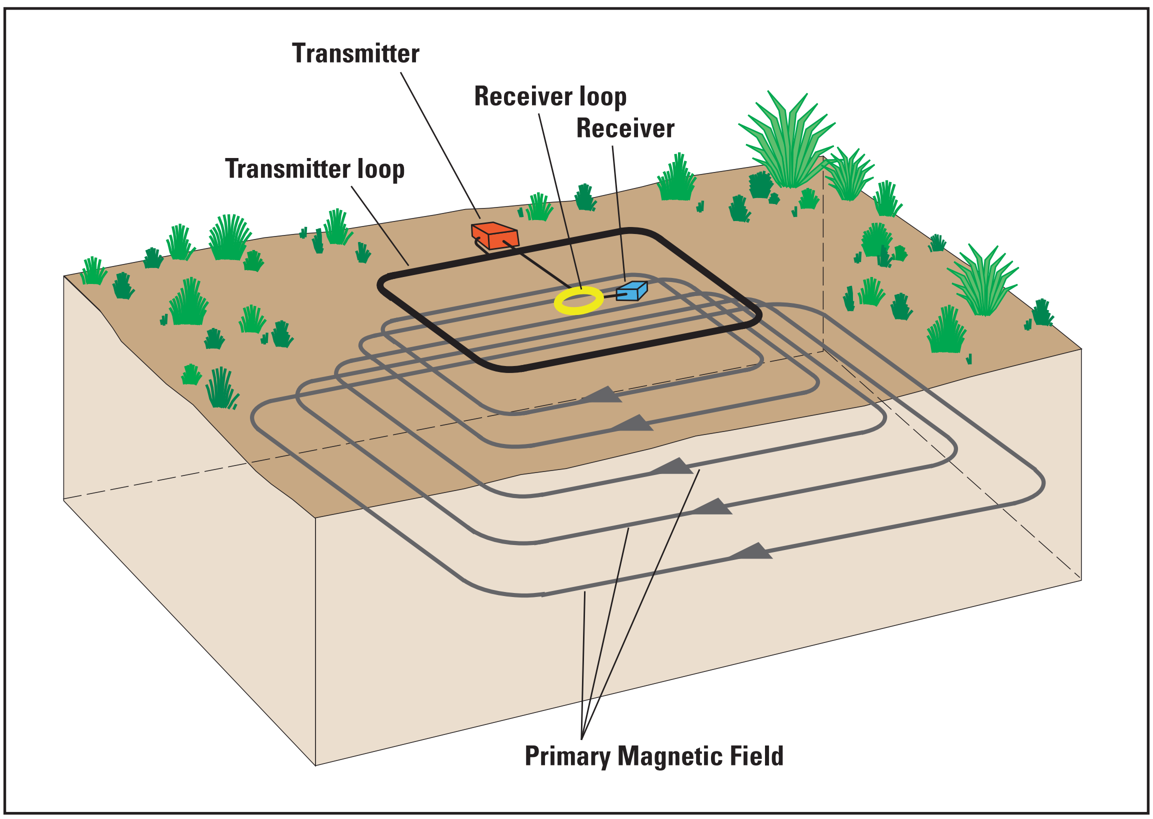

Figure 7. Diagram showing a transient electromagnetic (TEM) sounding layout and operation (modified from North Carolina Division of Water Resources, 2004).

Averaged data were imported into Zonge's STEMINV inversion software and PetRos EiKon EMIGMA software for 1-D inverse modeling. TEM sounding data were processed by forward simulation and inverse modeling using EMIGMA software (PetRos EiKon, Toronto, Canada), and by inverse modeling using Zonge's STEMINV. EMIGMA uses Occam and Marquart algorithms (PetRos EiKon, Toronto, Canada) to invert data so that calculated values are within 5 percent of observed data. Many models were examined before deciding on the final model.

TEM soundings were made in Nye County from April 29 to May 2, and from May 12 to 20, 2008. TEM soundings were made along the resistivity profile with the same north to south trend with a bend to the southwest on the lower half of the profile (fig. 5).

Controlled Source Audio Magnetotellurics (CSAMT)

CSAMT is a high-resolution electromagnetic sounding technique that uses a remote, grounded electric dipole transmitter as an artificial signal source (fig. 8). CSAMT is similar to the common audio-frequency magnetotelluric (AMT) geophysical techniques, except it uses an artificial source and, typically, higher frequencies. The transmitter source provides a stable signal, resulting in higher precision and faster measurements than what can be obtained from natural source AMT (Zonge, 1992).

CSAMT measurements typically are made at frequency ranges from 1 to 8,000 hertz in binary incremental steps and consist of orthogonal and parallel components of the electric (E) and magnetic (H) fields at a separation from 5 km to 15 km from the source (Sharma, 1997). CSAMT measurements can be taken in a number of different arrays depending on the type of information warranted. For widely spaced sounding or research-type applications, vector and tensor measurements are made using two electric-field components (Ex and Ey) and three magnetic-field components (Hx, Hy, and Hz). Another type of CSAMT array uses measurements made at electric and magnetic (Ex, Hy) receiving orthogonal pairs. For the purpose of this study, a "reconnaissance" type of CSAMT array was used, which consists of one electrical (Ex) and one magnetic (Hy) component for each measurement (Zonge, 1992). Multiple electrical fields are measured concurrently during reconnaissance CSAMT arrays, and this type of array also is referred to as controlled source audio-frequency electrotelluric (Zonge, 1992).

For the purpose of this study, a six-channel receiver was used, which had the capability of simultaneously measuring five electrical fields for every one magnetic field. The magnetic-field measurement is used to normalize the electrical fields and calculate the apparent resistivity and phase difference (Zonge, 1992). The variation in the magnetic field does not change much over the small area where the electric fields are measured and, therefore, can be measured more sparsely than the electrical fields. Grounded dipoles at the receiver site measure the electric field parallel to the transmitter (*Ex*), and a magnetic coil antenna senses the perpendicular magnetic field (*Hy*). The ratio of the Ex and Hy magnitudes yield the apparent resistivity (equation 3), also known as the Cagniard resistivity (Zonge, 1992):

$$\rho_a = 1/5f\,[Ex/Hy]^2 \qquad (3)$$

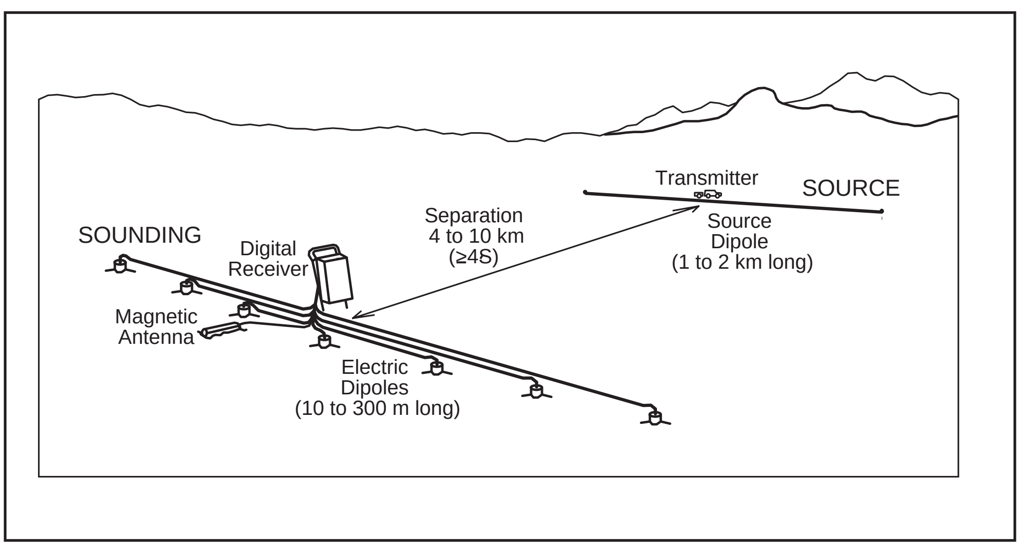

Figure 8. Diagram showing controlled source audio-frequency magnetotelluric (CSAMT) set-up (from Zonge, 1992).

where ρ_a is the apparent resistivity, *f* is the frequency, *Ex* is the electrical-field strength, and *Hy* is the magnetic-field strength.

The penetration of CSAMT into the subsurface and the depth of investigation is determined by the skin depth (equation 4):

$$S = 503 \sqrt{(\rho_a / f)} \quad (4)$$

where ρ_a is the measured apparent ground resistivity in ohm-m, and *f* is the signal frequency (Zonge, 1992). The skin depth is the depth at which the amplitude of a plane wave signal has dropped to 37 percent (1/e) of its value at the surface (Zonge, 1992). The skin depth is pertinent in CSAMT surveys because CSAMT data are most commonly interpreted by using simplified magnetotelluric (MT) equations, which are based on the assumption that the electrical and magnetic fields behave as plane waves. Unlike MT soundings, where the source is thought of as infinitely distant and nonpolarized, the CSAMT source is finite in distance and distinctly polarized (Sharma, 1997). The separation, r, between the transmitter and receiver for CSAMT surveys must be greater than three skin depths for the current driven into the ground to behave like plane waves (termed "far field"). When the separation is less than three skin depths at the frequency being measured, the electrical and magnetic fields change from plane-wave to curved ("near field"), and the equation for Cagniard resistivity no longer applies. CSAMT measurements from this study were examined for near- and far-field effects before modeling by plotting the apparent resistivity versus the frequency for a given set of soundings. All data from this study used for modeling are measured in the far field. A minimum separation between the source and receiver was 5 km, yielding a skin depth of greater than three (Zonge, 1992).

When the separation between the receiver and transmitter is greater than three skin depths, the equation for depth of investigation is (Zonge, 1992):

$$D = 356 \sqrt{(\rho_a / f)}. \quad (5)$$

The depth of investigation of a CSAMT survey can range from 20 to 3,000 m depending on the resistivity of the ground and the frequency of the signal. Typically, the source for a CSAMT survey should be separated from the survey line by about five times the depth of investigation. Therefore, if the maximum depth of investigation is 1 km, then the source should be placed about 5 km away.

CSAMT data were collected in Nye County from April 8 to 11, 21 to 24, and 28 to 29, 2008; May 21 to 22, 2008; and February 23 to 26, 2009, using a Zonge CSAMT acquisition system. The Zonge system consisted of a GDP-32II multichannel geophysical receiver connected to 6 electrical-sensing porous pots and a Zonge ANT3 high-gain mu-metal core magnetic antenna, a Zonge GGT-30 geophysical transmitter connected to a 25 kW trailer-mounted generator, and a Zonge XMT-32 transmitter controller. A 1-km-long bipole was used to transmit the electrical source, and 50 or 80 m dipoles were used to read each electrical field. CSAMT field setups consisted of one magnetic field with five accompanying electrical fields. CSAMT data were collected along the same profile as resistivity and TEM data. Five CSAMT lines were surveyed as a part of this project, Lines A, B, R, T, and W (fig. 5). Three different transmitter locations were used, but each transmitter location was unique to a specific line. No single CSAMT line had two transmitter locations and, therefore, a single Ex and Hy field were measured at each dipole for each line. The electrical fields for each line consisted of 80 m dipoles, except Lines A and B, which used 50 m dipoles.

Results

Results from the three techniques used in this study show an area of highly resistive material, hypothesized/presumed to be a Paleozoic limestone, in the area of Highway 95. The area of highly resistive material is faulted closer to the surface by the Highway 95 Fault than it is elsewhere in the area. Resistivity profiles between the three data sets show similar features, and those features are compared in the following sections.

Dipole-Dipole Direct-Current Resistivity Interpretations

DC resistivity data modeling consisted of calculating an apparent resistivity pseudosection, and an inverse resistivity model (figs. 9 and 10). The inverse model shows areas of greater resistivity from electrode positions 1 to 18 and areas of lower resistivity from electrodes 20 to 36 (fig. 10). The inverse model section shows a distinct change in resistivity between electrodes 18 and 20 (fig. 10). Measured topography was included in the inverse model to distinguish any topographic effects in the data, and none were observed (fig. 10). Areas with warm colors (yellow, orange, red) have high resistivity, and areas with cool colors (purple, blue, green) have low resistivity. The measured and calculated apparent resistivity pseudosections (fig. 9) and the inverse model section (fig. 10) show areas of high resistivity from electrode positions 1 to18, and a change to lower resistivity from electrode positions 20 to 34 (fig. 10). The high resistivity values between electrodes 1 to 14 from the land surface to an elevation of 400 m is interpreted as Paintbrush Group tuffs (figs. 10 and 11). These tuffs overlie a more conductive area that is interpreted as the Crater Flat Group tuffs and the Pre-Crater Flat Group tuffs (figs. 10 and 11). Between electrodes 14 and 20, at an elevation of 200 to 700 m, there is an area of resistive and conductive materials juxtaposed against each other that depicts the highly faulted nature of this part of the basin (fig. 10). DC resistivity modeling does not provide enough resolution to distinguish between faulted blocks, but it reinforces the interpretation that this area is not continuously horizontally layered earth. The inverse model shows a distinct change in resistivity near electrode positions 18 to 20, which is interpreted as the Highway 95 Fault (fig. 10). Resistive material (red) below an elevation of about 200 m between nodes 18 and 29 is interpreted as Paleozoic carbonate (fig. 10). Overlying the resistive material is a conductive layer, probably representing the saturated claystones and siltstones of the Pre-Crater Flat Group sedimentary rocks (blue to purple). Above the conductive unit, another resistive layer at the surface (red) probably is unsaturated alluvium (figs. 10 and 11).

Transient Electromagnetics Interpretations

TEM modeling consisted of calculating 1-D, smooth-model inversions of resistivity versus depth (figs. 12, 13, 14, and 15). The 1-D inversions are then interpolated to form a cross section of estimated resistivity with depth. Two types of TEM soundings were made in lower Fortymile Wash—500 m loop soundings and 150 m loop soundings.

Large TEM loops with 500 m sides were used to profile the subsurface to nearly 1.5 km, and smaller 150 m loops were used to profile the first 300 m of the subsurface. Two software packages were used for inversion of these data; Zonge STEMINV and PetRos EiKon EMIGMA.

Zonge STEMINV

TEM data were modeled first by using Zonge STEMINV. Inversion results from the 150 m loops produced models with two distinct layers and a transition zone between them (fig. 12). The upper most layer is resistive with values of about 100 ohm-m (yellow) and represents unsaturated Quaternary and Tertiary alluvium (figs. 11 and 12). At an elevation of about 725 m, resistivity becomes more conductive (yellow to green) which possibly delineates the water level (fig. 12). The water level appears slightly deeper in the northern part of the plot compared to the southern part, but only by about 20 m, and that may be due to resolution in the modeling. The transition between the two layers lies between 725 and 600 m elevation (fig. 12). Resistivity values in this transition change from about 100 ohm-m at 725 m elevation to about 16 ohm-m near 600 m elevation (fig. 12). The transition represents the change associated with saturated sediments and underlying Crater Flat Group tuffs (fig. 11). Below the transition is a conductive second layer (blue) with resistivity values ranging from 3 to 10 ohm-m, probably representing the Crater Flat Group tuffs and the saturated claystones and siltstones of the Pre-Crater Flat Group sedimentary rocks (figs. 11 and 12). In the northern part of the plot, between stations 101 and 109, moderately resistive material alternates from north to south with conductive material (fig. 12). Bottoms of the inverse models are where the colored resistivity plot ends abruptly (fig. 12).

Inversions results from the 500 m loops also produced results with two distinct layers (fig. 13). The upper most layer is resistive (yellow) with values of 100 ohm-m or more. At an elevation of about 725 m, there is a transition to more conductive units (green to blue), possibly representing the water table. At an elevation of about 600 m, there is a distinct change to even more conductive material (blue), about 6 ohm-m, which represents the underlying Crater Flat Group tuffs and the Pre-Crater Flat Group sedimentary rocks (figs. 11 and 13). Near station 206 and 211, there are indications of more resistive material at depth (green to yellow), assumed to be the Paleozoic carbonate units, but the inverse models produced by this software do not extend into the resistive material.

PetRos EiKon EMIGMA

TEM data also were modeled using PetRos EiKon EMIGMA software. Inversion results were similar to the results from the Zonge software with a layering of resistive over conductive material (fig. 14). Inversions from EMIGMA produced 3 distinct layers from the TEM soundings. The uppermost layer consists of about 75 m of resistive material, assumed to be dry Quaternary and Tertiary alluvium (red), ranging from the land surface to an elevation of about 725 m (figs. 11 and 14). The second layer is a slightly less resistive layer (yellow to green) with resistivity values ranging from 75 to 240 ohm-m (fig. 14). The expected water level is near this depth (Nuclear Waste Repository Project Office, 2009), and the change in resistivity between 700 and 725 m elevation is interpreted as being the transition into saturated sediments (fig. 14). At an elevation of 600 m, there is a distinct change in resistivity to a conductive unit (blue to purple; fig. 14). The conductive material probably represents the younger sedimentary rocks and the claystone and siltstone Pre-Crater Flat Group sedimentary rocks (fig. 11).

Inversion results from the 500 m loops obtained by using EMIGMA were comparable to inversion results obtained by using the Zonge software, but EMIGMA results identify the deep resistive Paleozoic Carbonate that the Zonge software failed to identify (fig. 15). Near the surface there is resistive material (yellow), about 200 to 300 ohm-m, and it extends to an elevation of 730 m. Below the resistive material is a conductive unit (blue to purple) that extends from 700 m elevation to about 330 m elevation. The conductive units represent the Crater Flat Group Tuffs and the Pre-Crater Flat Group sedimentary rocks (figs. 11 and 15). Inversion results from the EMIGMA software identified resistive materials (green to red) at an elevation below 330 m that represent the Paleozoic carbonate uplifted by the Highway 95 Fault (figs. 11 and 15).

Controlled Source Audio Magnetotelluric Interpretations

Five lines of CSAMT data were collected in lower Fortymile Wash to better characterize the Highway 95 Fault

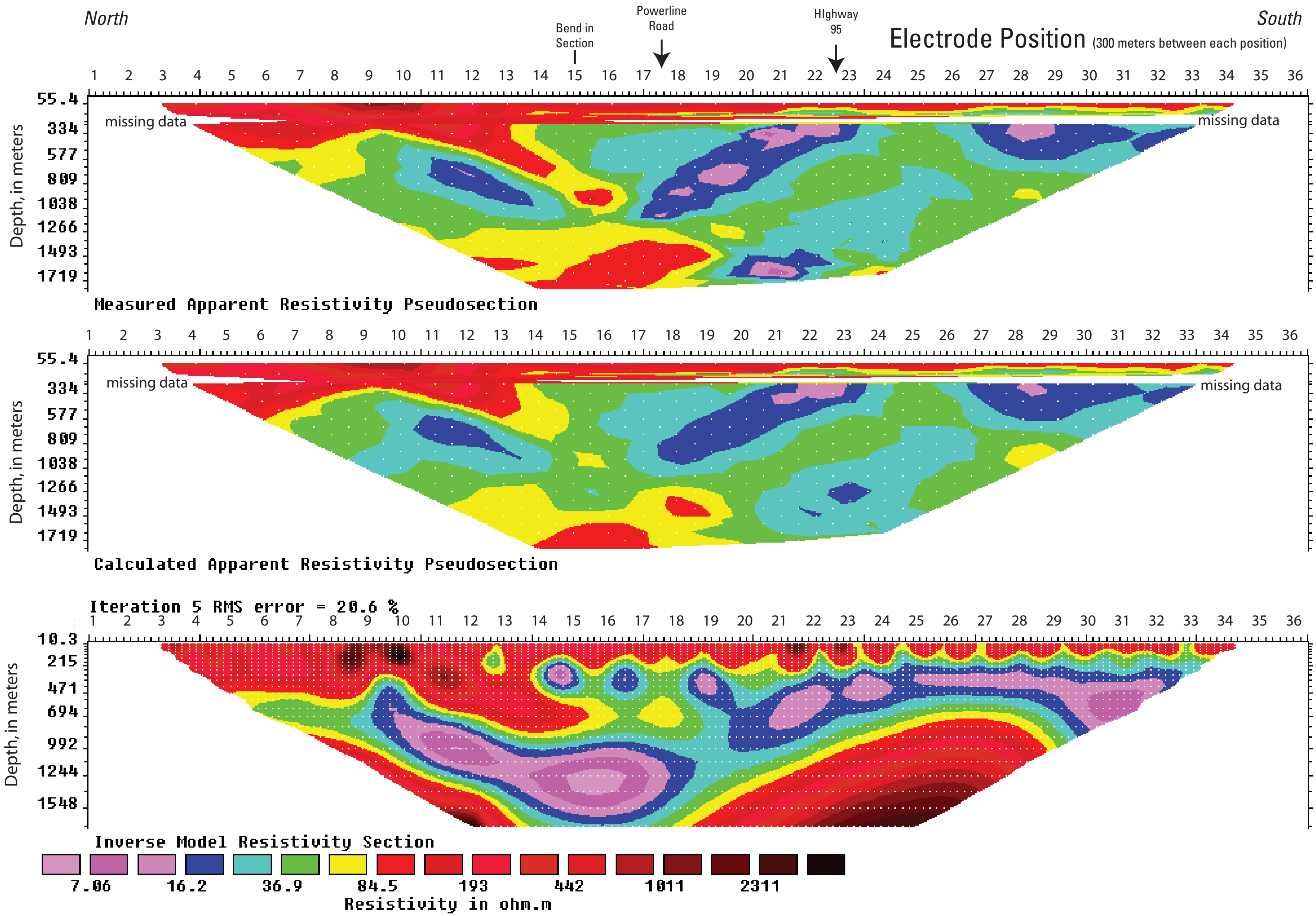

Figure 9. Measured apparent resistivity pseudosection, calculated apparent resistivity pseudosection, and inverse model resistivity section without compensated topography. Areas with warm colors (yellow, orange, red) have high resistivity, and areas with cool colors (purple, blue, green) have low resistivity.

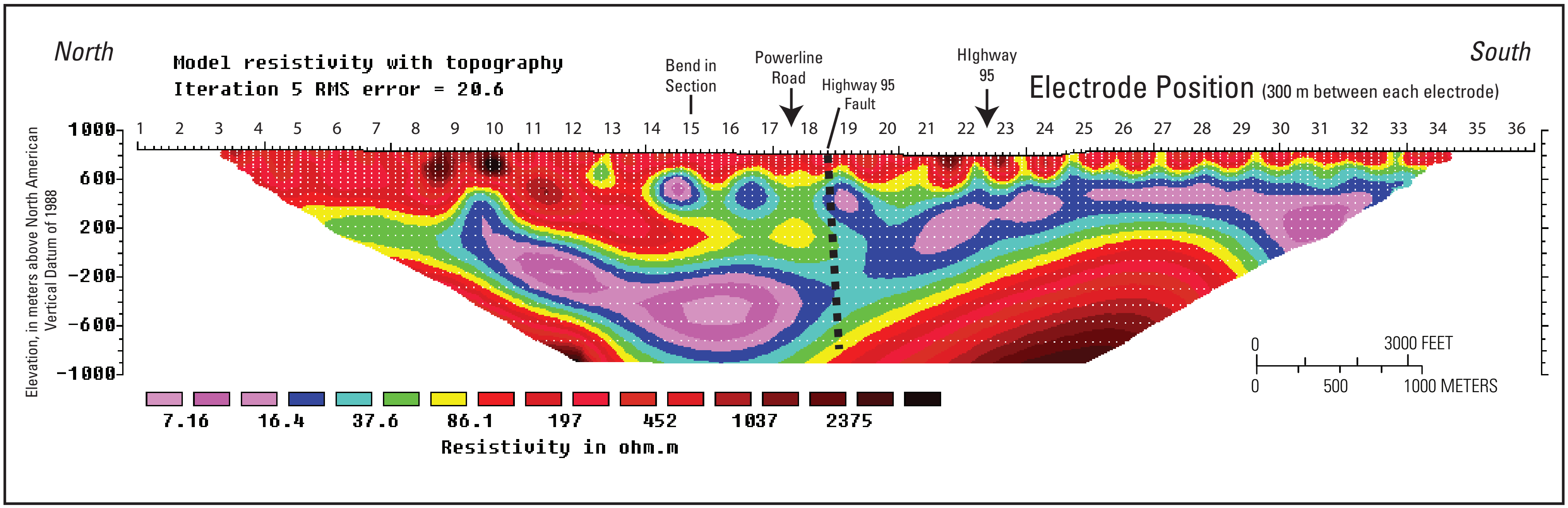

Figure 10. Inverse model resistivity section from dipole-dipole direct current resistivity survey. RMS is the root-mean-square difference between the measured and calculated apparent resistivities and is used to determine the accuracy of the model.

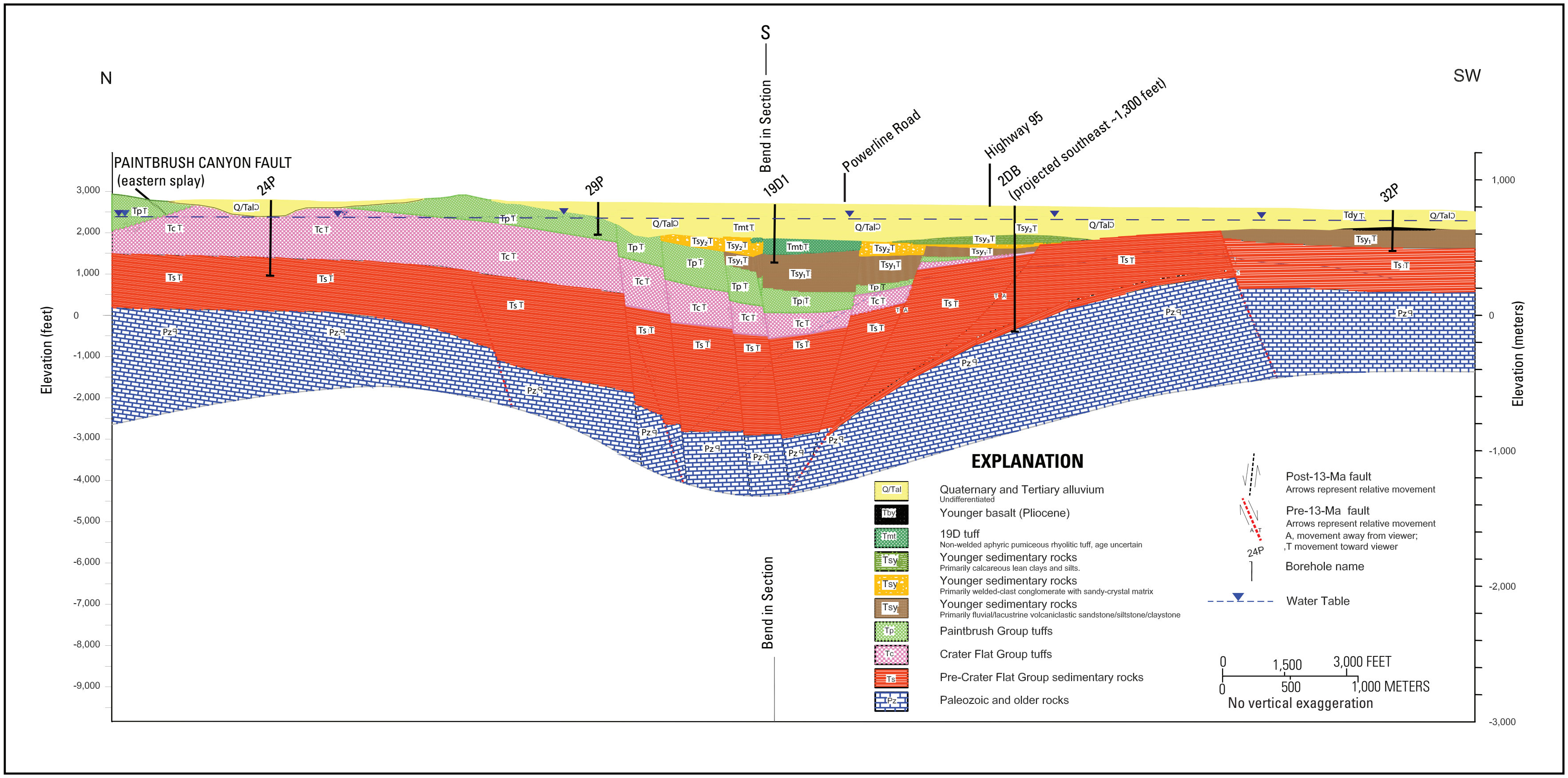

Figure 11. Interpreted geologic cross section of the transect that includes the dipole-dipole resistivity profile, the 150 m and 500 m transient electromagnetic profiles, and Line R from the controlled source audio-frequency magnetotelluric profiles (modified from Nuclear Waste Repository Project Office, 2009).

(Lines A, B, R, T, and W; fig. 5). Interpretations of CSAMT data for this project are more detailed than the other geophysical techniques because measurement locations were more closely spaced and provided a greater density of data for modeling. Line A trends from north to south and begins near electrode 11 of the resistivity profile (fig. 5). Inversion results from Line A show four distinct layers (fig. 16). From the land surface to an elevation of about 775 m there is a highly resistive layer (red to yellow) with resistivity values ranging from about 20 ohm-m to about 300 ohm-m (fig. 16). The resistive material represents unsaturated Quaternary and Tertiary alluvium (fig. 11). The second layer is a mixture of resistive and conductive material (blue to yellow-green with some red) found between elevations 775 m and 575 m with resistivity values ranging from 10 ohm-m to about 300 ohm-m (fig. 16). There are many resistive areas (red) within the second layer, and that could be attributable to faulting within the basin that juxtaposes blocks of resistive material next to conductive material. The resistive material in the second layer may represent Tertiary Paintbrush Group tuffs with possible faulted blocks of more conductive younger sedimentary rocks (fig. 11). The uppermost conductive material of the second layer also can represent saturated overlying Quaternary alluvium. The third layer for Line A is very conductive material (blue to purple) ranging from 3 to 10 ohm-m (fig. 16). This layer is not very thick and can be found between elevations 575 m and 475 m (fig. 16). The conductive material probably represents the Crater Flat Group tuffs (fig. 11). The fourth and final layer of Line A is a mixture of conductive and moderately conductive material (green to blue-purple) representing the Pre-Crater Flat Group tuffs (figs. 11 and 16). This layer extends from about 475 m elevation to below mean sea level and outside of our depth of investigation (fig. 11).

Line B is another north to south trending CSAMT survey, and it is similar to the interpretation of Line A (fig. 2). Inversion results from Line B are represented in the subsurface as four layers, and the beginning of the Highway 95 Fault

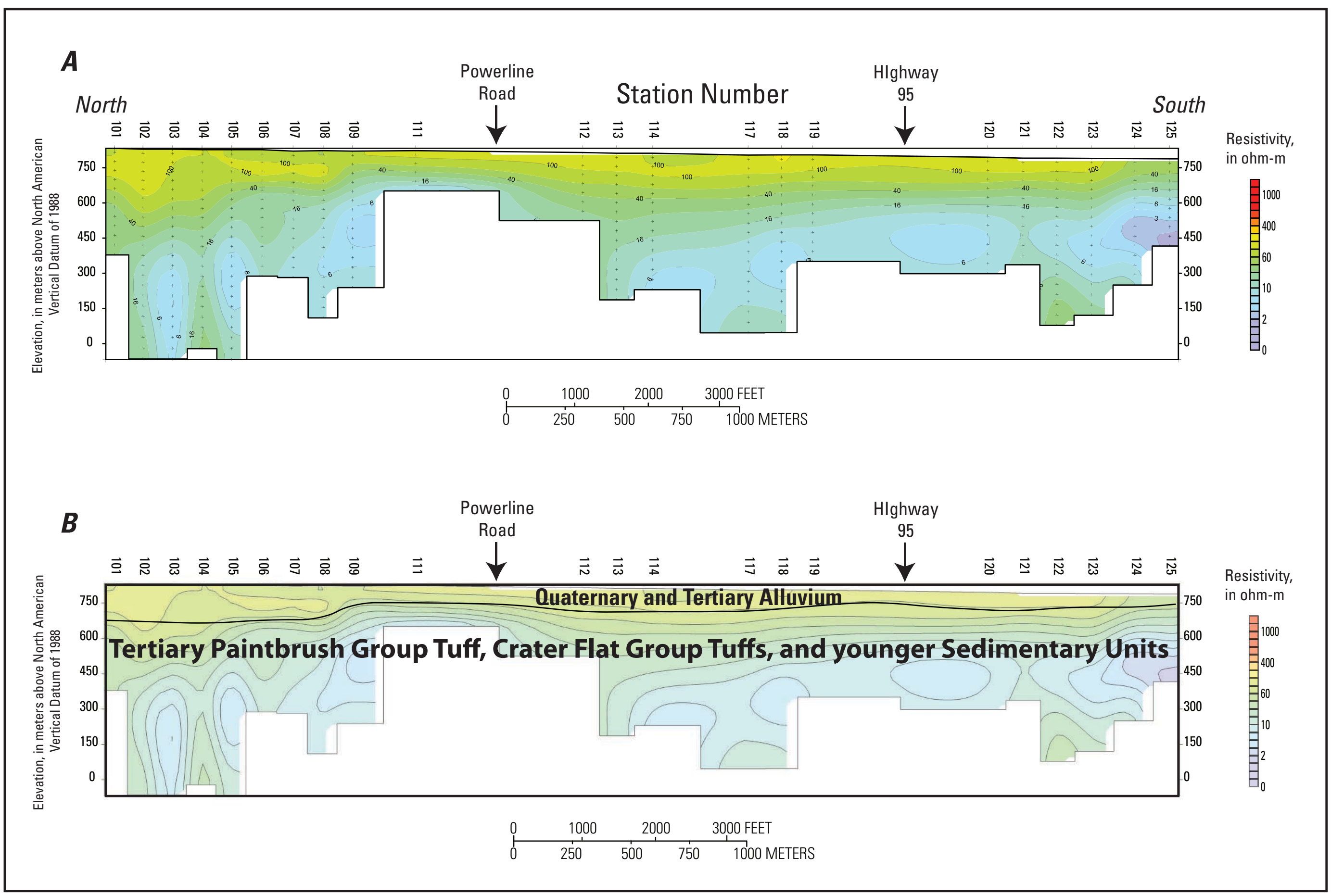

Figure 12. *A*, North to south cross section (see fig. 2) of transient electromagnetic, smooth-model inversion results for 150 m loops using Zonge STEMINV modeling software. *B*, Interpretations of inversion results for 150 m loops using Zonge STEMINV modeling software. The blocky white area at the bottom of the plots are areas where the inverse models did not extend deeper into the subsurface.

is observed in the Line B inversion (fig. 17). From the land surface to an elevation of about 775 m there is a more resistive layer (red to yellow) with resistivity values ranging from about 20 ohm-m to about 400 ohm-m (fig. 17). The resistive material represents unsaturated Quaternary and Tertiary alluvium. The second layer consists of both resistive and conductive materials (yellowish-lighter green and dark green-blue) found between elevations 775 m and 575 m with resistivity values ranging from 10 ohm-m to about 400 ohm-m (fig. 17). There is much faulting in this part of the basin, and resistive Paintbrush Group tuffs are juxtaposed against younger sedimentary fluvial, lacustrine, volcaniclastic sandstones, siltstones, and claystones (Nuclear Waste Repository Project Office, 2009). The alternating resistive and conductive material in the geophysical section probably represents that faulting (fig. 11). A third highly conductive layer (blue) with resistivity values between 3 and 16 ohm-m can be found between elevations of 575 m and 400 m representing the Crater Flat Group tuffs (figs. 11 and 17). The fourth layer from the inversion of Line B is a moderately conductive layer (yellowish-green to blue-purple) that extends from 400 m to the bottom of the plot near mean sea level (fig. 17). At the southern part of the section, near stations 3775 to 4125 and an elevation of 0 to 50 m, there is resistive material (orange) ranging from 40 to 200 ohm-m (fig. 17). This material could be Paleozoic carbonate that is faulted upward by the Highway 95 Fault (figs. 11 and 17). This is the first glimpse in

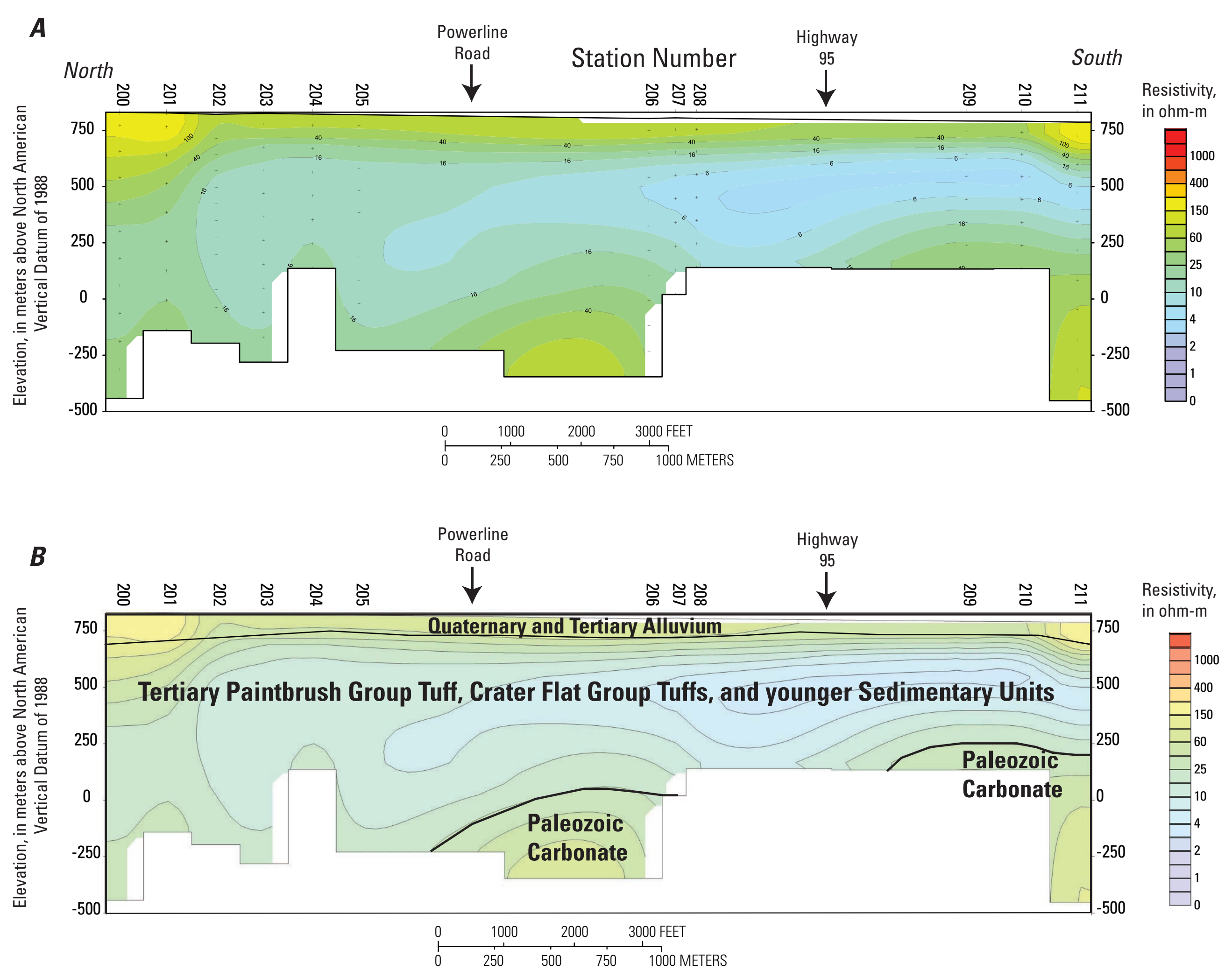

Figure 13. *A*, North to south cross section of transient electromagnetic, smooth-model inversion results for 500 m loops using Zonge STEMINV modeling software. *B,* Interpretations of inversion results for 500 m loops using Zonge STEMINV modeling software. The blocky white area at the bottom of the plots are areas where the inversion models did not extend deeper into the subsurface.

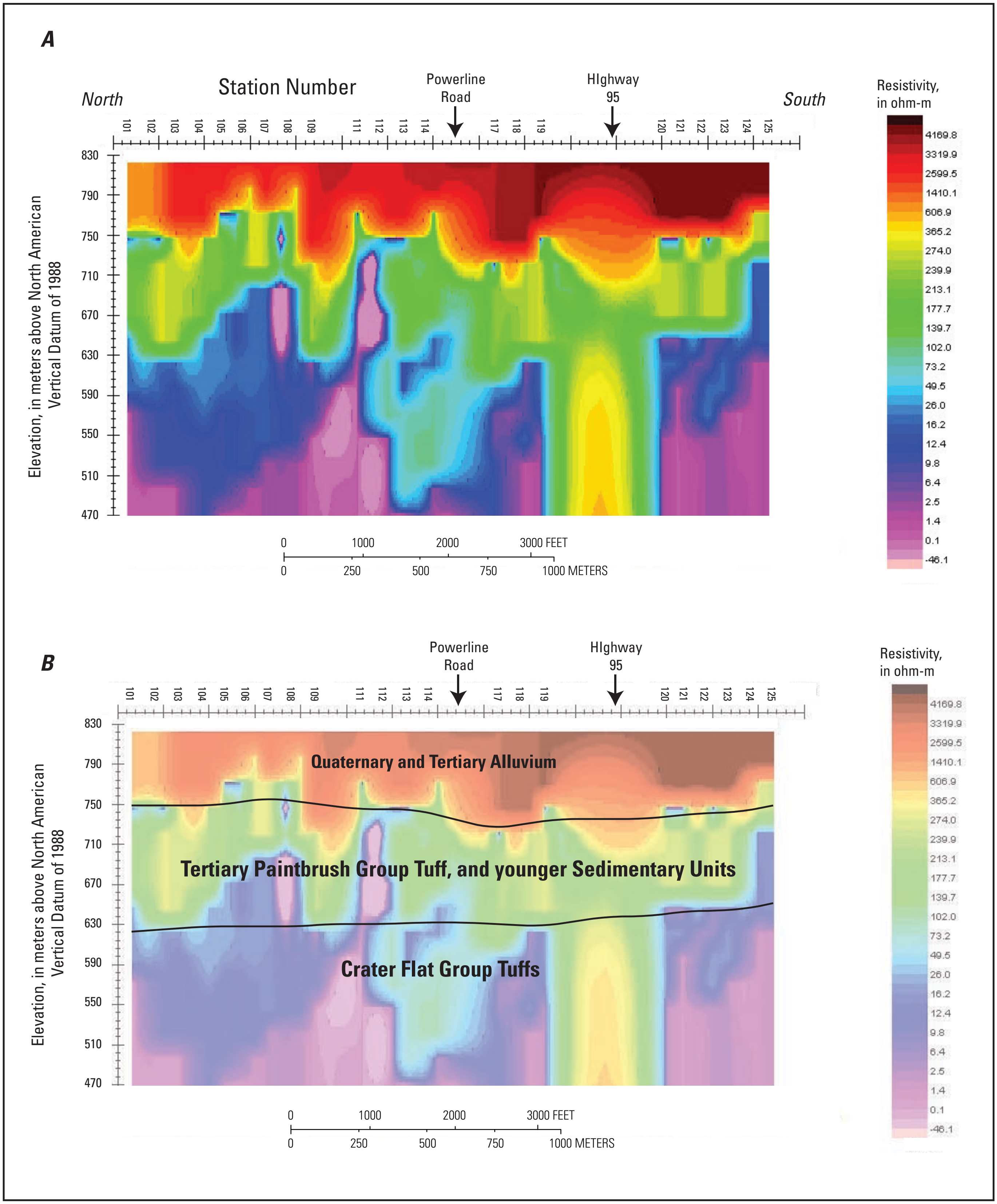

Figure 14. *A*, North to south cross section of transient electromagnetic, smooth-model inversion results for 150 m loops using PetRos Eikon EMIGMA modeling software. *B*, Interpretations from inversion results for 150 m loops using EMIGMA modeling software.

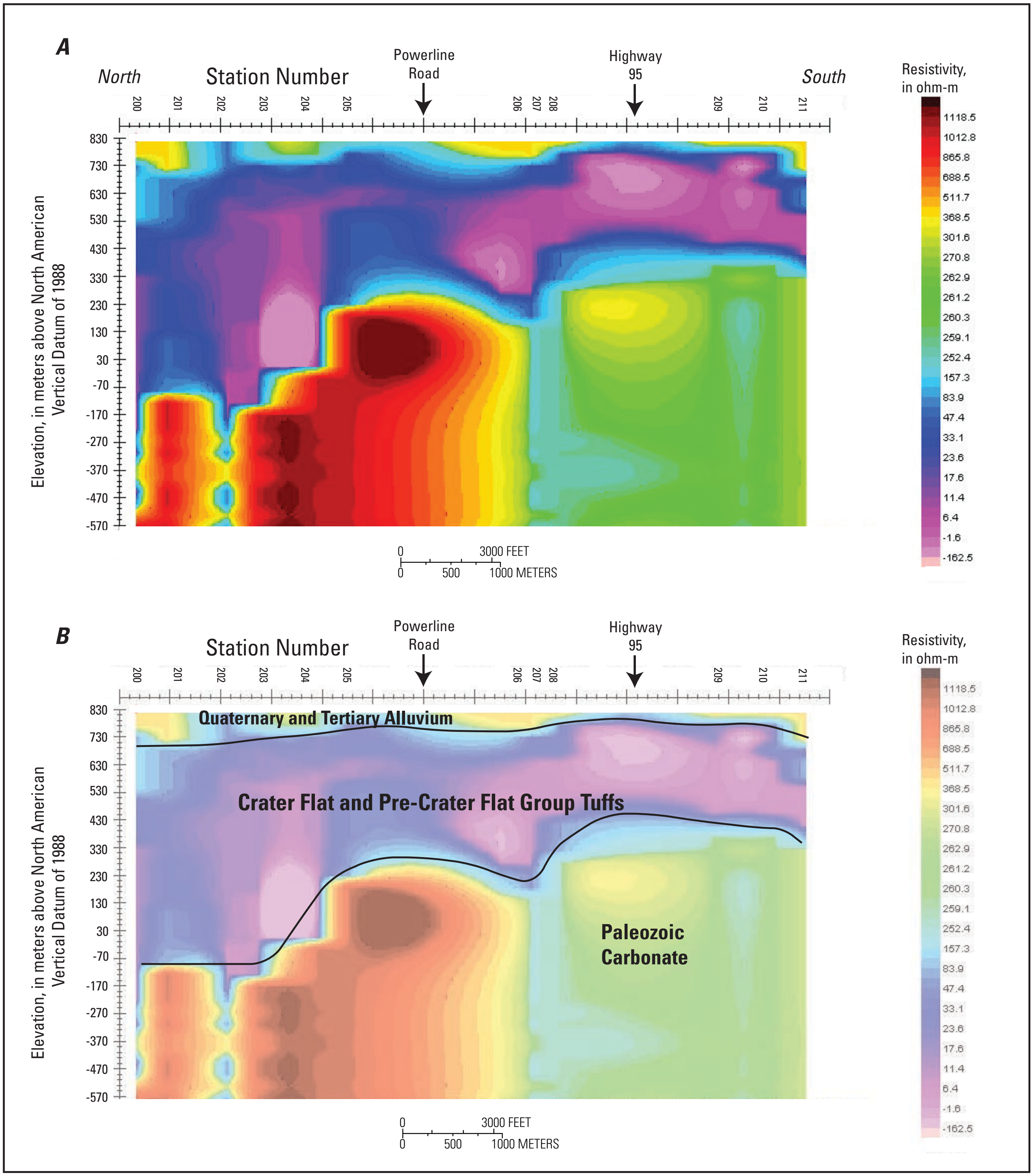

Figure 15. *A*, North to south cross section of transient electromagnetic, smooth-model inversion results for 500 m loops using PetRosEikon EMIGMA modeling software. *B*, Interpretations of inversion results for 500 m loops using PetRos Eikon EMIGMA modeling software.

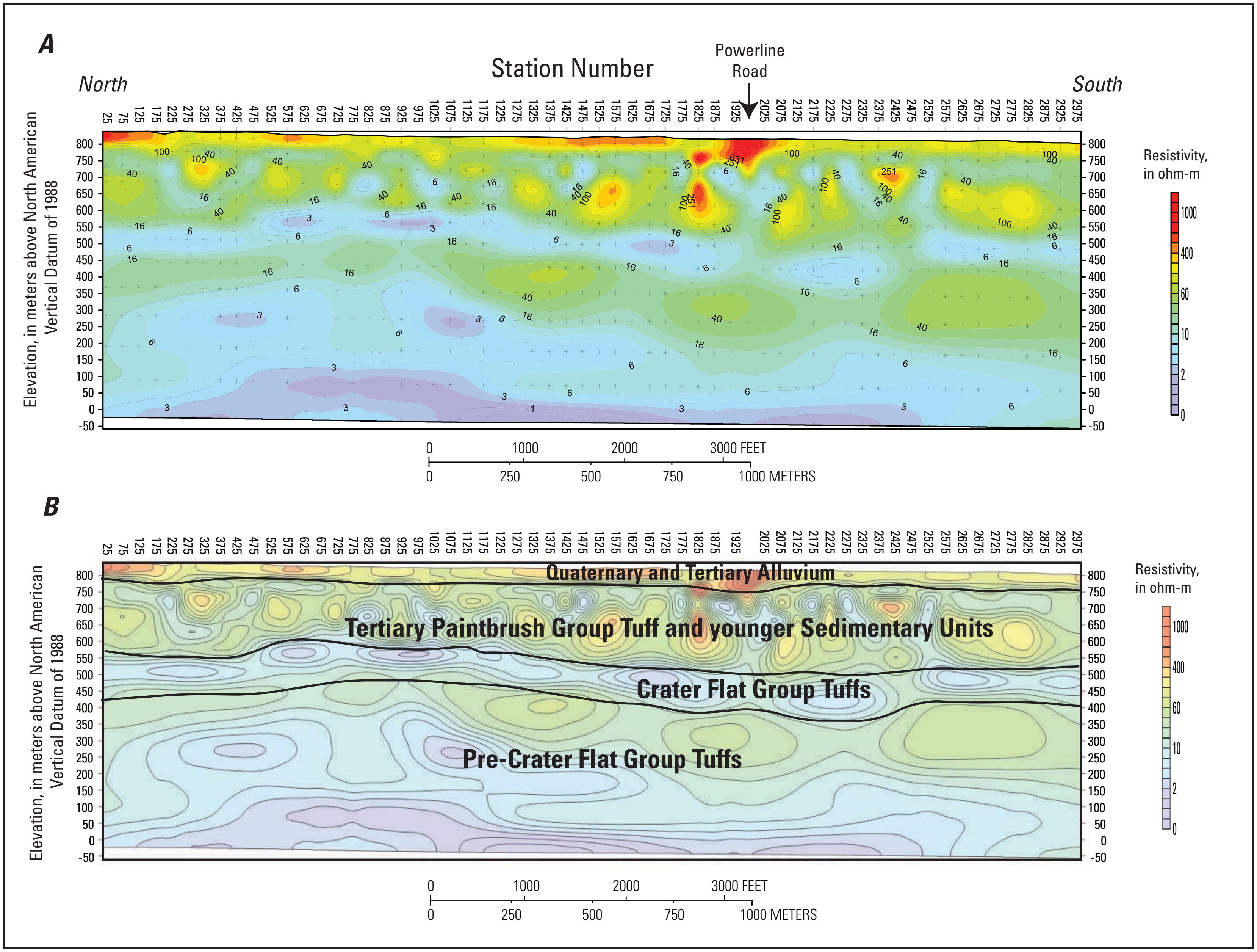

Figure 16. *A*, North to south cross section of controlled source audio-frequency magnetotelluric, smooth-model inversion results for Line A. *B*, Interpretations of inversions results for Line A.

the modeling of resistive material at depth associated with the Highway 95 Fault, and it will be furthered explored in the rest of the CSAMT plots.

The longest of the five CSAMT surveys is Line R, and it extends over much of the length of the dipole-dipole resistivity line, including the bend in the southern half of the line which may distort some of the modeling results (fig. 5). The northern portion of Line R is in the same area as Lines A and B and has similar features to both. The upper most layer (yellowish-green to red), from the land surface to about 775 m elevation, is Quaternary and Tertiary alluvium (fig. 18). The second layer is a combination of resistive and conductive material (10 to 300 ohm-m) that represents the faulted blocks of Paintbrush Group and Crater Flat Group tuffs (figs. 11 and 18). The more conductive material (blue to purple) underlying the Paintbrush Group is the Pre-Crater Flat Group of sedimentary rocks that was observed juxtaposed against more resistive material (yellow-green to orange) near station 3800 (figs. 11 and 18). The Highway 95 Fault is evident toward the southern part of this plot where resistive material (100 to 400 ohm-m; yellow-green to red) is adjacent to conductive material (1 to 10 ohm-m; blue-purple; fig. 18). Inversions from Line R show a distinct resistivity change near station 3800, which is thought to be the Highway 95 Fault (fig. 18). The resistive material represents Paleozoic carbonates that are uplifted to an elevation of about 490 m. A more conductive material (blue to purple) overlies the carbonate and represents the Pre-Crater Flat Group of sedimentary rocks (figs. 11 and 18). The upper most 100 m above the sedimentary rocks is another layer of slightly more resistive material (yellowish-green) which represents the Quaternary and Tertiary alluvium (fig. 11). Based on interpretation from NWRPO, the Highway 95 Fault may inhibit shallow groundwater movement by uplifting deep Paleozoic carbonates, effectively reducing the overlying alluvial aquifer thickness and restricting the movement of water. Upward vertical hydraulic gradients in wells proximal to the fault indicate that upward cross-formational movement is occurring from deeper higher pressure aquifers.

To verify the spatial occurrence of the Highway 95 Fault, two additional CSAMT lines (Lines T and W) were surveyed to the east of Line R in the same northeast to southwest direction as the lower portion of Line R (fig. 2). Line T starts on the Nevada National Security Site at the same latitude as electrode 14 from the dipole-dipole resistivity survey (figs. 1 and 2). Inversions from Line T showed variable results including unexpected areas of anomalously high resistivity near the surface between stations 920 and 1400 (fig. 19). The uppermost layer of the rest of Line T, from land surface to 750 m elevation, is a moderate to highly resistive area with resistivity values between 40 and 3,000 ohm-m, and it is interpreted as unsaturated Quaternary alluvium (figs. 11 and 19). Between elevations of 750 m to 320 m, there is a layer of alternating resistive and conductive materials ranging from 3 to 600 ohm-m (fig. 19). The Post-Crater Flat Group faulting could account for the alternating blocks of resistive and conductive material (fig. 11). Below an elevation of 320 m, there is a more conductive unit ranging from 1 to 16 ohm-m, which represents the Pre-Crater Flat Group of sedimentary rocks (figs. 11 and 19). South of station 3480, a more resistive unit of about 100 ohm-m is interpreted as the Paleozoic Carbonate uplifted by the Highway 95 Fault (figs. 11 and 19). The conductive material near station 2900, adjacent to the resistive material near station 3480, represents the Highway 95 Fault (fig. 19).

Line W, named for Washburn Road, parallels Line T and the southern part of Line R (fig. 2). Inversions from Line W show resistive Quaternary and Tertiary alluvium from the land surface to an elevation of 775 m (fig. 20). Below the alluvium in the northern part of the plot, between stations 440 and 1160, are conductive and resistive materials ranging from 6 to 250 ohm-m at an elevation of 775 to 240 m (fig. 20). The range in resistivity values (6 to 250 ohm-m) probably represents the faulted blocks of resistive Paintbrush Group tuffs and conductive younger sedimentary rocks (figs. 11 and 20). Below 240 m elevation is a conductive unit ranging from 3 to 16 ohm-m, and it is interpreted as Pre-Crater Flat Group tuffs (figs. 11 and 20). Near station 1960, in the central part of the survey, there is a distinct change in resistivity at depth (fig. 20). The change near station 1960 is interpreted as the Highway 95 Fault, and uplifted Paleozoic Carbonates are visible with resistivity values ranging from 40 to 100 ohm-m (figs. 11 and 20). The Paleozoic Carbonate is interpreted to be between elevations 400 and -80 m (fig. 20). Overlying the carbonate is a conductive unit, Pre-Crater Flat Group sedimentary rocks that range between 6 and 16 ohm-m (figs. 11 and 20). Above these conductive sedimentary rocks, there is a gradual transition to more resistive overlying alluvium with resistivity values between 40 and 100 ohm-m (fig. 20).

CSAMT Lines A, B, R, T, and W were plotted using ESRI's Arc Scene, 3-dimensional visualizing software, to look at the spatial extent of the Highway 95 Fault and the variability between CSAMT survey lines (figs. 21, 22, and 23). A view to the northwest of the inverted CSAMT resistivity sections shows the Highway 95 Fault at, or just north of, Highway 95 in the vicinity of Line R (fig. 21). Moving to the southwest, the Highway 95 Fault is south of Highway 95 as shown in Lines T and W (fig. 21). Turning the view to the northeast reveals the beginnings of the Highway 95 Fault in Line B (fig. 22). The Highway 95 Fault is located just south of Highway 95 near Line B (fig. 22). Continuing to turn the view to the east reveals the Highway 95 Fault on Lines A, R, T, and W (fig. 23). The Highway 95 Fault, appropriately named, uplifts more resistive material at, or south of, Highway 95, as indicated by the 3-dimensional views.

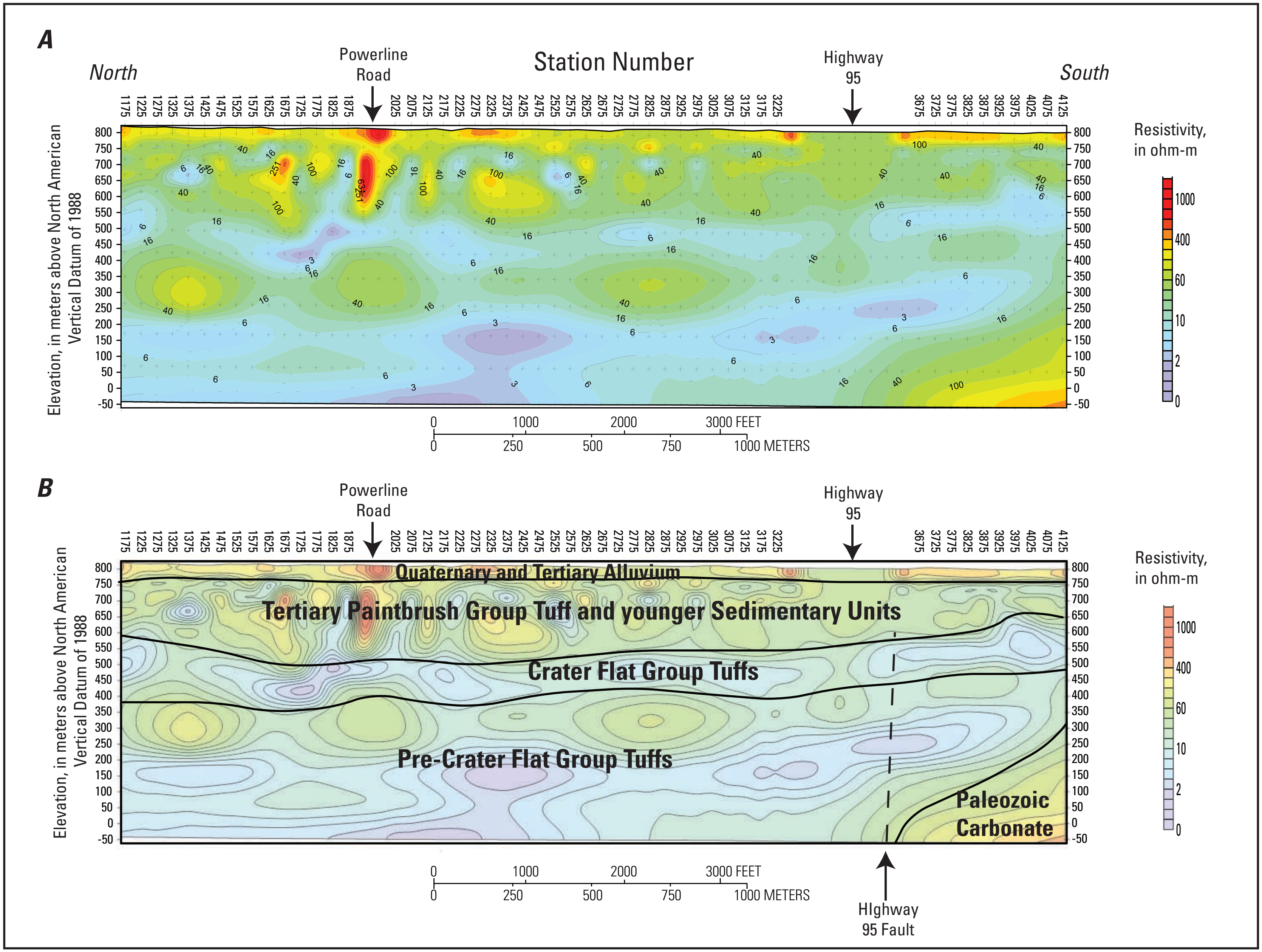

Figure 17. *A*, North to south cross section of controlled source audio-frequency magnetotelluric, smooth-model inversion results for Line B. *B*, Interpretations of inversions results for Line B.

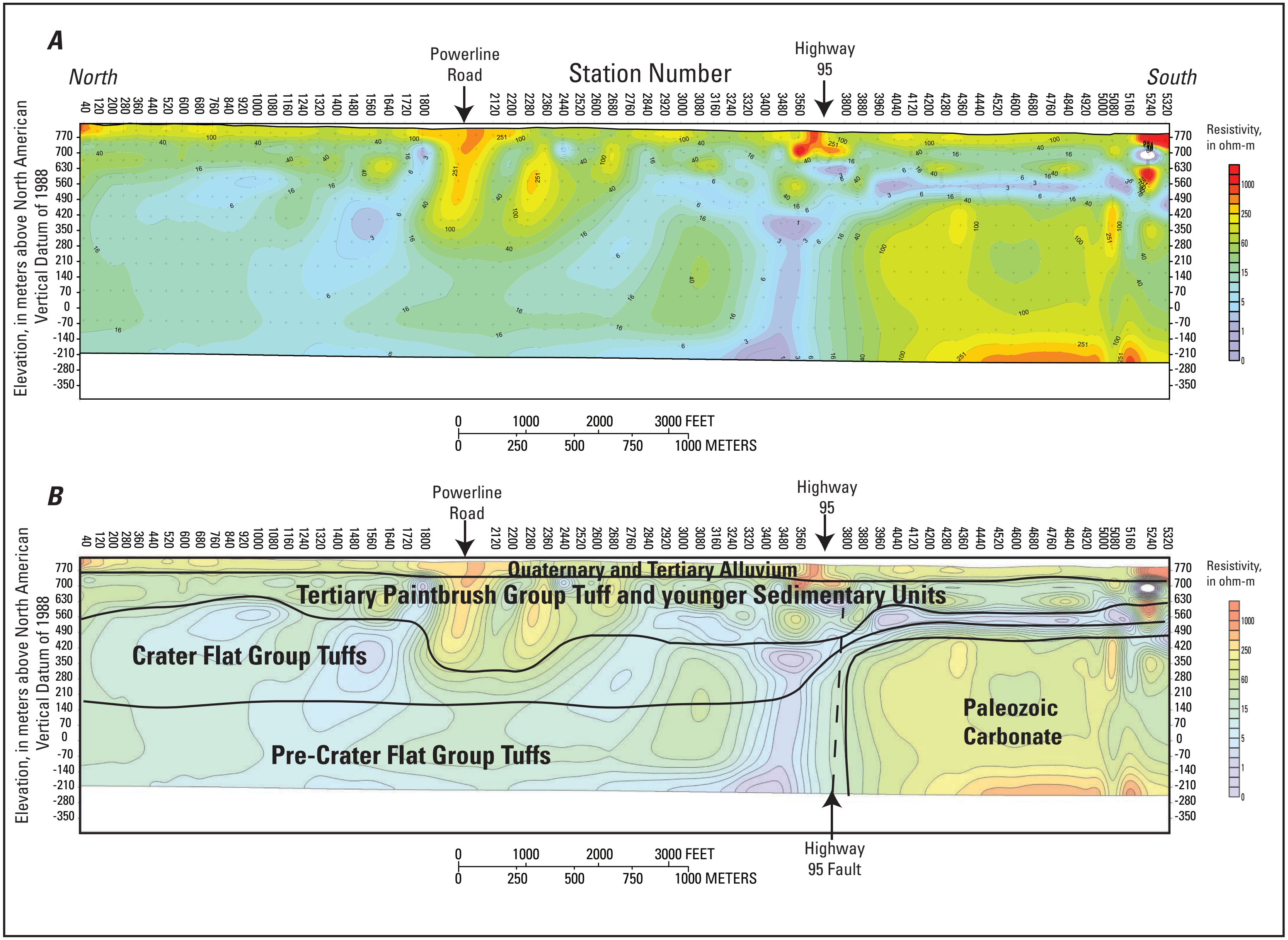

Figure 18. *A,* North to south cross section of controlled source audio-frequency magnetotelluric, smooth-model inversion results for Line R. *B,* Interpetations of inversion results for Line R.

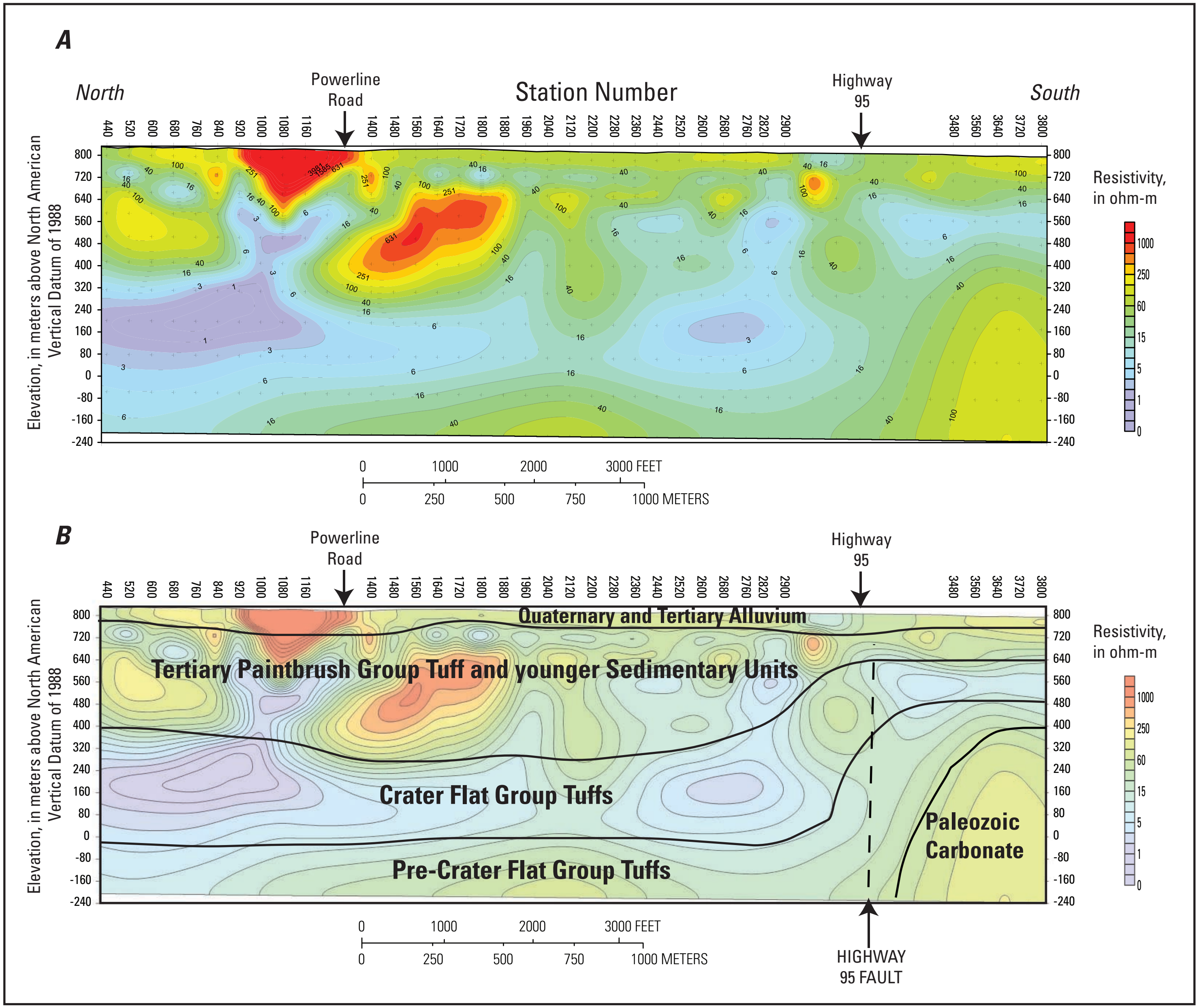

Figure 19. *A*, North to south cross section of controlled source audio-frequency magnetotelluric, smooth-model inversion results for Line T. *B*, Interpretations of inversion results for Line T.

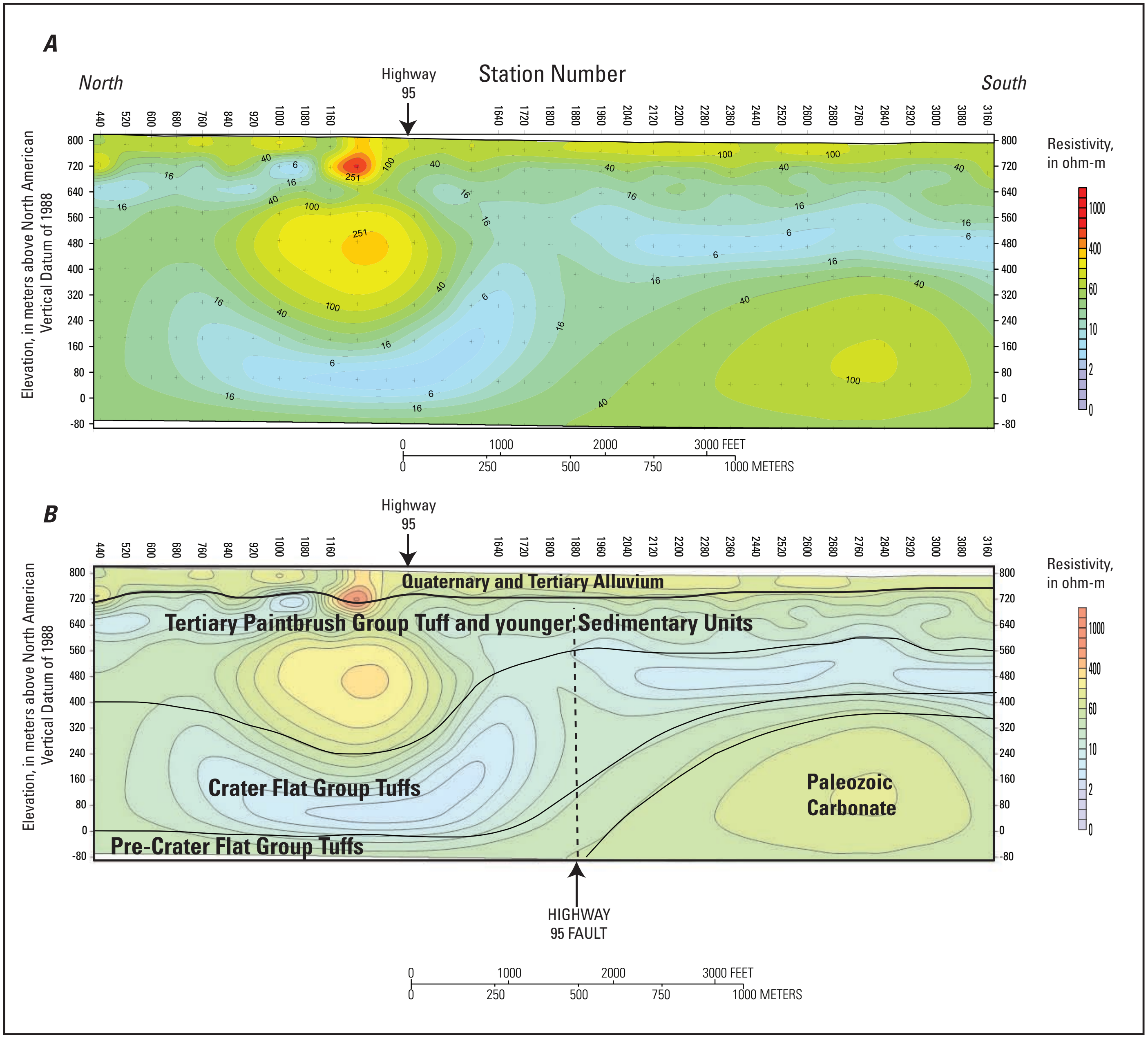

Figure 20. *A*, North to south cross section of controlled source audio-frequency magnetotelluric, smooth-model inversion results for Line W. *B,* Interpretations of inversion results for Line W.

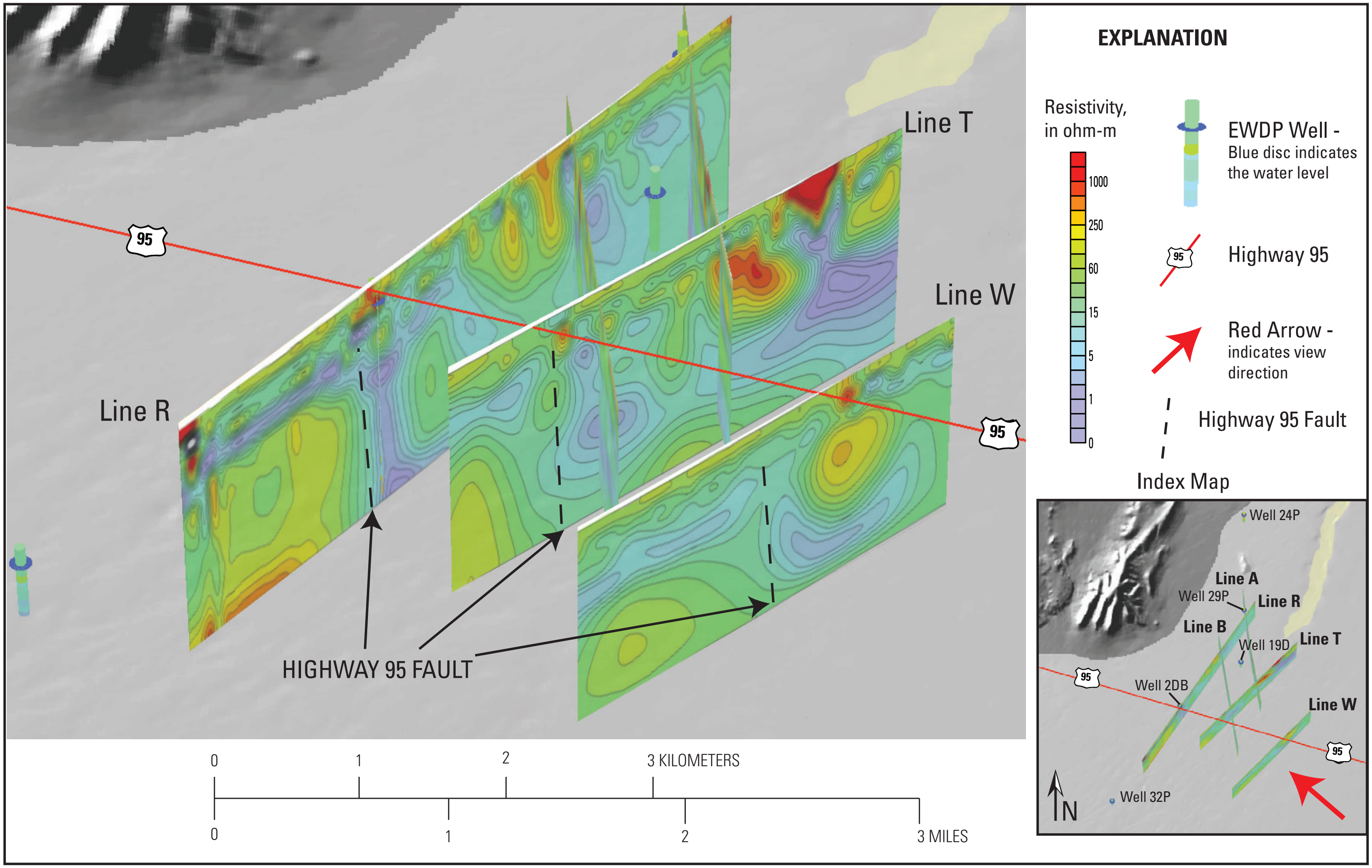

Figure 21. View to the northwest of inverted resistivity sections from CSAMT surveys in lower Fortymile Wash, Nye County, Nevada.

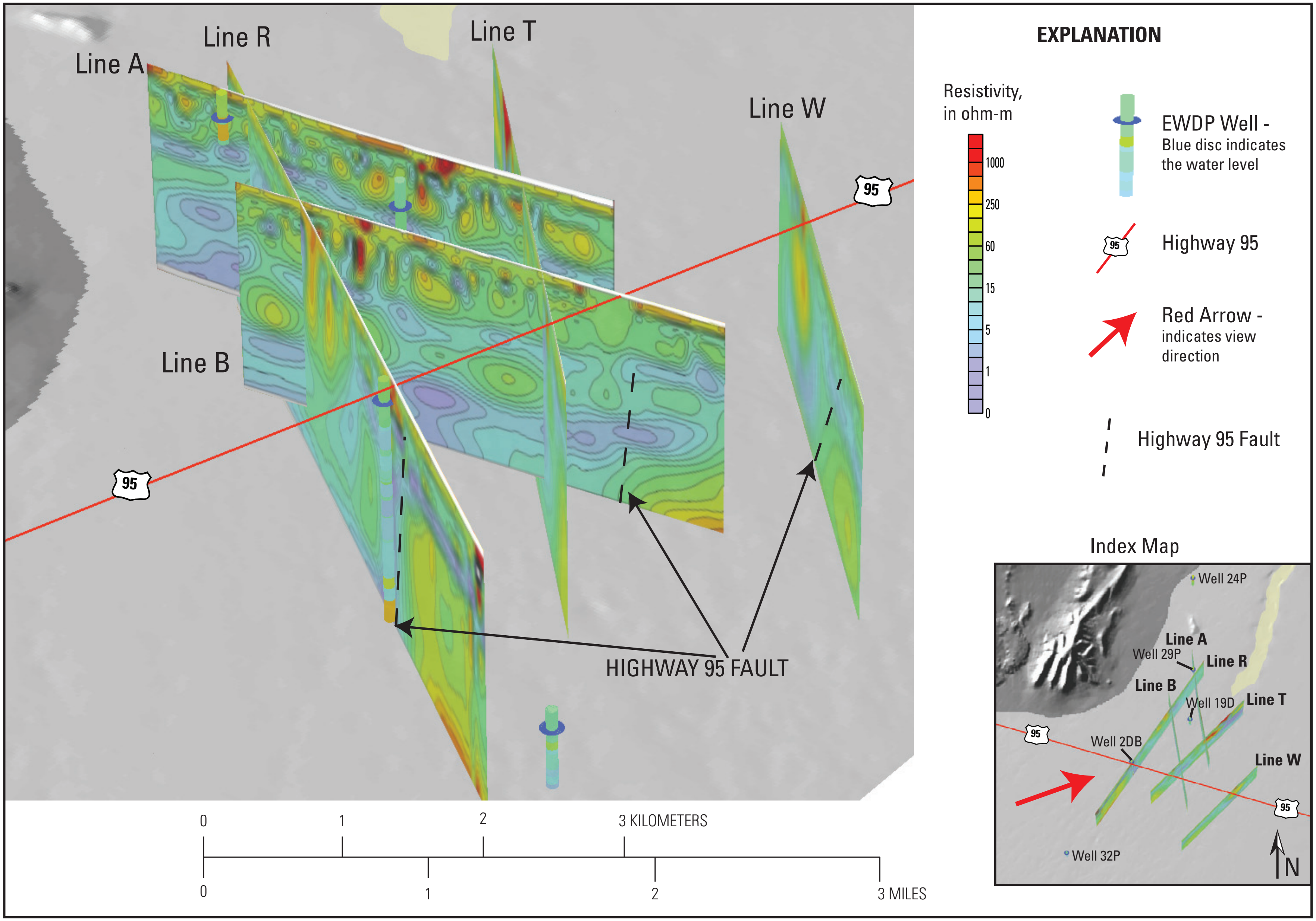

Figure 22. View to the northeast of inverted resistivity sections from CSAMT surveys in lower Fortymile Wash, Nye County, Nevada.

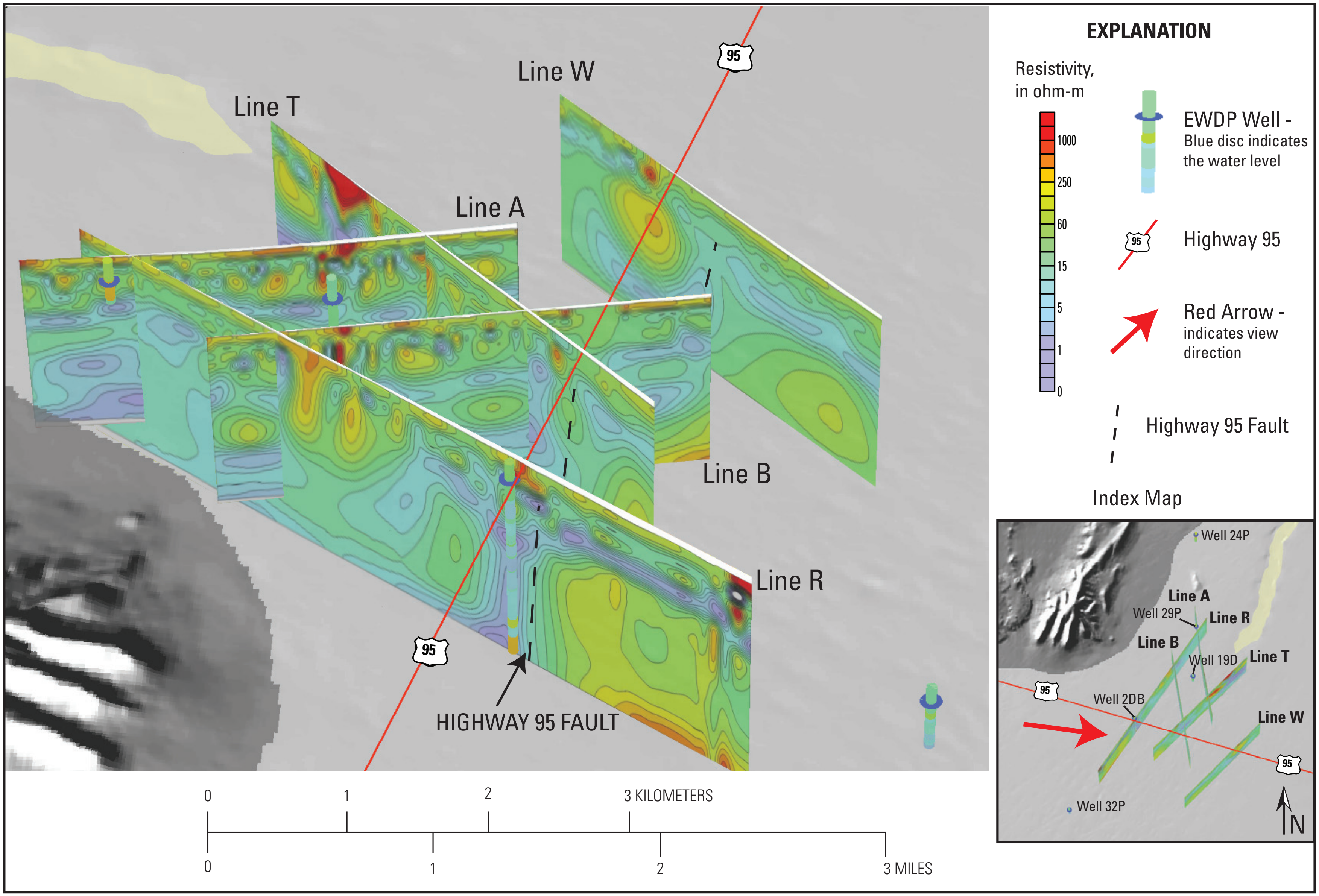

Figure 23. View to the east of inverted resistivity sections from CSAMT surveys in lower Fortymile Wash, Nye County, Nevada.

Conclusions

The USGS AZWSC, in cooperation with Nye County, has used dipole-dipole DC resistivity, TEM, and CSAMT to better understand the Highway 95 Fault. The Highway 95 Fault is a buried, roughly east-west trending growth fault at the southern extent of Yucca Mountain and the Southwestern Nevada Volcanic Field. Results indicate that the fault is just north of U.S. Highway 95, between wells NC-EWDP-2DB and -19D in the vicinity of dipole-dipole resistivity profile, the TEM transects, and CSAMT Line R. Results also indicate that the Highway 95 Fault is approximately 300 m south of Highway 95, east of NC-EWDP-2DB, in the vicinity of CSAMT Lines T and R. The Highway 95 Fault may inhibit shallow groundwater movement by uplifting deep Paleozoic carbonates, effectively reducing the overlying alluvial aquifer thickness and restricting the movement of water. Upward vertical hydraulic gradients in wells proximal to the fault indicate that upward movement is occurring from deeper, higher pressure aquifers.

Coordinated application of electrical and electromagnetic geophysical methods provided better characterization of the Highway 95 Fault than that provided by existing borehole data. The comparison of dipole-dipole resistivity, TEM, and CSAMT data support the interpretation of faulting of an uplifted block of resistive Paleozoic carbonate that lies beneath a more conductive sandstone unit. A more resistive alluvial basin-fill unit is found above the sandstone unit and comprises about 150 m of the uppermost subsurface.

References Cited

Fitterman, D.V., and Stewart, M.T., 1986, Transient electromagnetic sounding for groundwater: Geophysics, vol. 51, no. 4, p. 995-1005.

Fridrich, C.J., 1999, Tectonic evolution of the Crater Flat Basin, Yucca Mountain Region, Nevada, *in* Wright, L.A., and Troxel, B.W., eds., Cenozoic basins of the Death Valley Region: Geological Society of America Special Paper 333.

Hallof, P.G., 1992, Electrical—IP and Resistivity, *in* Van Blaricom, R., ed., Practical geophysics II for the exploration geologist: Northwest Mining Association, 137 p.

Nabighian, M.N., and Macnae, J.C., 1987, Time domain electromagnetic prospecting methods, *in* Nabighian, M.N., ed., Electromagnetic methods in applied geophysics, v. 2: Tulsa, Oklahoma, Society of Exploration Geophysics.

North Carolina Division of Water Resources, 2004, Time domain electromagnetic geophysics, accessed June 16, 2010, at http://www.ncwater.org/Education_and_Technical_Assistance/Ground_Water/TDEM/.

Nuclear Waste Repository Project Office, 2009, Nye County Early Warning Drilling Program Phase V Report, Technical Report No. NWRPO-2009-02: Pahrump, Nevada, Nuclear Waste Repository Project Office.

Palacky, G.J., 1987, Resistivity characteristics of geologic targets, chap. 3 *of* Nabighian, M.N., ed., Electromagnetic methods in applied geophysics–Volume 1, Theory: Tulsa, Okla., Society of Exploration Geophysicists, Investigations in Geophysics no. 3.

Potter, C.J., Dickerson, R.P., Sweetkind, D.S., Drake, R.M., Taylor, E.M., Fridrich, C.J., San Juan, C.A., and Day, W.C., 2002, Geologic map of the Yucca Mountain region, Nye County, Nevada: U.S. Geological Survey Geologic Investigations Series I–2755, 1:50,000 scale, 44-p. pamphlet.

Sharma, P.V., 1997, Environmental and engineering geophysics: Cambridge, Cambridge University Press.

Sumner, J.S., 1976, Principles of induced polarization for geophysical exploration: New York, Elsevier Scientific Publishing Company, 277 p.

Telford, W.M., Geldart, L.P., and Sheriff, R.E., 1976, Applied geophysics: New York, Cambridge University Press, 770 p.

U.S. Department of Energy, 2007, Draft Supplemental Environmental Impact Statement for a Geologic Repository for the Disposal of Spent Nuclear Fuel and High-Level Radioactive Waste at Yucca Mountain, Nye County, Nevada, Volume 1–Impact analyses, chap. 3–Affected environment, fig. 3-13, Revised potentiometric surface map for the Yucca Mountain area: U.S. Department of Energy.

Workman, J.B., Menges, C.M., Page, W.R., Taylor, E.M., Bartlett, E.E., Rowley, P.D., Dixon, G.L., Thompson, R.A., and Wright, L.A., 2002, Geologic map of the Death Valley ground-water model area, Nevada and California: U.S. Geological Survey Miscellaneous Field Studies Map MF-2381-A, 1:250,000, 26-p. pamphlet.

Yungul, S.H., 1996, Electrical methods in geophysical exploration of deep sedimentary basins: New York, Chapman and Hall, 208 p.

Zohdy, A.A.R., Eaton, G.P., and Mabey, D.R., 1974, Application of surface geophysics to ground-water investigations: U.S. Geological Survey Techniques of Water-Resources Investigations, book 2, Chap. D1, 116 p.

Zonge, K., 1992, Broad band electromagnetic systems, *in* Van Blaricom, R., ed., Practical geophysics II for the exploration geologist: Northwest Mining Association, 96 p.

This page intentionally left blank.

Appendix 1

Appendix 1. Location of Dipole-Dipole Direct Current Resistivity Electrodes, Transient Electromagnetic Soundings, and Controlled Source Audio-Frequency Magnetotelluric Electrodes

Appendix 1-1. Location of each dipole-dipole resistivity electrode.

[Coordinate system: Universal Transverse Mercator Zone 11, North American Datum of 1983; elevation is in meters above the North American Vertical Datum of 1988]

Electrode identifier	Easting (meters)	Northing (meters)	Elevation (meters)
Electrode 1	4063197	549271	847
Electrode 2	4062897	549320	846
Electrode 3	4062597	549320	845
Electrode 4	4062297	549320	845
Electrode 5	4061997	549320	845
Electrode 6	4061696	549206	845
Electrode 7	4061395	549143	842
Electrode 8	4061095	549090	839
Electrode 9	4060795	549089	836
Electrode 10	4060508	549218	836
Electrode 11	4060196	549306	834
Electrode 12	4059896	549341	832
Electrode 13	4059596	549350	829
Electrode 14	4059297	549320	827
Electrode 15	4058997	549301	825
Electrode 16	4058738	549206	821
Electrode 17	4058500	549052	816
Electrode 18	4058265	548843	813
Electrode 19	4058047	548604	811
Electrode 20	4057849	548341	807
Electrode 21	4057643	548174	805
Electrode 22	4057393	547816	801
Electrode 23	4057249	547468	799
Electrode 24	4056990	547351	797
Electrode 25	4056796	547292	794
Electrode 26	4056561	547174	830
Electrode 27	4056331	546993	830
Electrode 28	4056158	546695	830
Electrode 29	4055973	546407	830
Electrode 30	4055776	546177	830
Electrode 31	4055554	546015	830
Electrode 32	4055282	545874	830
Electrode 33	4055062	545761	830
Electrode 34	4054758	545573	830
Electrode 35	4054485	545358	830
Electrode 36	4054350	545066	830

Appendix 1-2. Location of the center of each 150 m TEM sounding loop.

[Coordinate system: Universal Transverse Mercator Zone 11, North American Datum of 1983; elevation is in meters above the North American Vertical Datum of 1988]

Loop identifier	Easting (meters)	Northing (meters)	Elevation (meters)
Loop 100	549210	4060266	833
Loop 101	549215	4060127	829
Loop 102	549228	4059977	829
Loop 103	549236	4059831	827
Loop 104	549246	4059683	827
Loop 105	549253	4059533	827
Loop 106	549252	4059384	821
Loop 107	549259	4059235	823
Loop 108	549279	4059084	821
Loop 109	549256	4058936	822
Loop 110	549258	4058790	823
Loop 111	549177	4058597	818
Loop 112	548805	4058223	815
Loop 113	548700	4058117	812
Loop 114	548585	4058004	812
Loop 115	548477	4057901	808
Loop 116	548377	4057804	804
Loop 117	548272	4057707	804
Loop 118	548160	4057605	805
Loop 119	548052	4057512	805
Loop 120	547430	4056996	795
Loop 121	547396	4056844	791
Loop 122	547357	4056701	791
Loop 123	547307	4056561	790
Loop 124	547213	4056401	789
Loop 125	547115	4056285	788

Appendix 1-3. Location of the center of each 500 m TEM sounding loop.

[Coordinate system: Universal Transverse Mercator Zone 11, North American Datum of 1983; elevation is in meters above the North American Vertical Datum of 1988]

Loop identifier	Easting (meters)	Northing (meters)	Elevation (meters)
Loop 200	549060	4060078	831
Loop 201	549054	4059839	828
Loop 202	549047	4059586	822
Loop 203	549053	4059337	826
Loop 204	549046	4059085	823
Loop 205	549056	4058837	820
Loop 206	548080	4057921	803
Loop 207	547993	4057836	806
Loop 208	547916	4057772	804
Loop 209	547044	4056899	792
Loop 210	546946	4056669	791
Loop 211	546853	4056438	787

Appendix 1-4. Receiver Station Location of each CSAMT electrode for Line A.

[Coordinate system: Universal Transverse Mercator Zone 11, North American Datum of 1983; elevation is in meters above the North American Vertical Datum of 1988]

Electrode identifier	Easting (meters)	Northing (meters)	Elevation (meters)
Electrode 0	549288	4060317	838
Electrode 50	549294	4060272	837
Electrode 100	549297	4060222	837
Electrode 150	549298	4060172	839
Electrode 200	549305	4060121	830
Electrode 250	549314	4060078	840
Electrode 300	549316	4060027	837
Electrode 350	549324	4059979	836
Electrode 400	549329	4059930	835
Electrode 450	549336	4059881	837
Electrode 500	549341	4059829	836
Electrode 550	549350	4059778	830
Electrode 600	549354	4059728	828
Electrode 650	549357	4059679	829
Electrode 700	549367	4059627	826
Electrode 750	549372	4059578	829
Electrode 800	549379	4059536	826
Electrode 850	549385	4059487	826

Appendix 1-4. Receiver Station Location of each CSAMT electrode for Line A.—Continued

[Coordinate system: Universal Transverse Mercator Zone 11, North American Datum of 1983; elevation is in meters above the North American Vertical Datum of 1988]

Electrode identifier	Easting (meters)	Northing (meters)	Elevation (meters)
Electrode 900	549391	4059437	823
Electrode 950	549398	4059387	824
Electrode 1000	549403	4059339	823
Electrode 1050	549407	4059290	822
Electrode 1100	549415	4059241	822
Electrode 1150	549421	4059191	823
Electrode 1200	549429	4059142	823
Electrode 1250	549436	4059092	823
Electrode 1300	549443	4059043	822
Electrode 1350	549451	4058994	821
Electrode 1400	549458	4058944	820
Electrode 1450	549465	4058896	817
Electrode 1500	549472	4058846	821
Electrode 1550	549480	4058797	823
Electrode 1600	549489	4058748	820
Electrode 1650	549498	4058698	821
Electrode 1700	549505	4058648	824
Electrode 1750	549512	4058600	818
Electrode 1800	549521	4058551	816
Electrode 1850	549531	4058502	816
Electrode 1900	549540	4058455	815
Electrode 1950	549549	4058403	816
Electrode 2000	549558	4058355	816
Electrode 2050	549566	4058307	815
Electrode 2100	549575	4058258	816
Electrode 2150	549584	4058210	814
Electrode 2200	549594	4058161	814
Electrode 2250	549603	4058113	814
Electrode 2300	549612	4058064	812
Electrode 2350	549621	4058016	812
Electrode 2400	549630	4057968	812
Electrode 2450	549639	4057919	811
Electrode 2500	549648	4057871	811
Electrode 2550	549658	4057818	810
Electrode 2600	549668	4057769	809
Electrode 2650	549677	4057720	809
Electrode 2700	549687	4057672	811
Electrode 2750	549695	4057623	811

Appendix 1-4. Receiver Station Location of each CSAMT electrode for Line A.—Continued

[Coordinate system: Universal Transverse Mercator Zone 11, North American Datum of 1983; elevation is in meters above the North American Vertical Datum of 1988]

Electrode identifier	Easting (meters)	Northing (meters)	Elevation (meters)
Electrode 2800	549704	4057576	807
Electrode 2850	549714	4057525	807
Electrode 2900	549725	4057478	804
Electrode 2950	549734	4057429	804
Electrode 3000	549743	4057381	801

Appendix 1-5. Receiver station location of each CSAMT electrode for Line B.

[Coordinate system: Universal Transverse Mercator Zone 11, North American Datum of 1983; elevation is in meters above the North American Vertical Datum of 1988]

Electrode identifier	Easting (meters)	Northing (meters)	Elevation (meters)
Electrode 1150	548678	4059190	822
Electrode 1200	548687	4059140	818
Electrode 1250	548697	4059090	817
Electrode 1300	548706	4059043	818
Electrode 1350	548714	4058995	815
Electrode 1400	548721	4058944	813
Electrode 1450	548730	4058895	813
Electrode 1500	548739	4058847	816
Electrode 1550	548749	4058797	815
Electrode 1600	548757	4058747	817
Electrode 1650	548767	4058698	811
Electrode 1700	548774	4058649	812
Electrode 1750	548783	4058600	814
Electrode 1800	548792	4058550	813
Electrode 1850	548801	4058501	813
Electrode 1900	548809	4058453	814
Electrode 2000	548827	4058359	811
Electrode 2050	548832	4058306	808
Electrode 2100	548841	4058258	809
Electrode 2150	548848	4058208	812
Electrode 2200	548858	4058159	806
Electrode 2250	548866	4058110	813
Electrode 2300	548876	4058061	811
Electrode 2350	548885	4058013	812

Appendix 1-5. Receiver station location of each CSAMT electrode for Line B.—Continued

[Coordinate system: Universal Transverse Mercator Zone 11, North American Datum of 1983; elevation is in meters above the North American Vertical Datum of 1988]

Electrode identifier	Easting (meters)	Northing (meters)	Elevation (meters)
Electrode 2400	548894	4057963	811
Electrode 2450	548901	4057914	811
Electrode 2500	548911	4057865	810
Electrode 2550	548918	4057816	808
Electrode 2600	548927	4057768	809
Electrode 2650	548934	4057719	807
Electrode 2700	548944	4057669	804
Electrode 2750	548949	4057621	810
Electrode 2800	548958	4057574	810
Electrode 2850	548965	4057523	810
Electrode 2900	548974	4057476	809
Electrode 2950	548982	4057426	808
Electrode 3000	548991	4057375	811
Electrode 3050	548997	4057328	811
Electrode 3100	549007	4057278	807
Electrode 3150	549014	4057229	805
Electrode 3200	549023	4057176	808
Electrode 3250	549031	4057131	803
Electrode 3650	549099	4056742	801
Electrode 3700	549107	4056690	805
Electrode 3750	549115	4056641	804
Electrode 3800	549119	4056590	802
Electrode 3850	549129	4056541	800
Electrode 3900	549137	4056493	799
Electrode 4000	549152	4056396	797
Electrode 4050	549163	4056345	800
Electrode 4100	549171	4056296	799
Electrode 4150	549180	4056248	800

Appendix 1-6. Receiver station location of each CSAMT electrode for Line R.

[Coordinate system: Universal Transverse Mercator Zone 11, North American Datum of 1983; elevation is in meters above the North American Vertical Datum of 1988]

Electrode identifier	Easting (meters)	Northing (meters)	Elevation (meters)
Electrode 0	549293	4060241	832
Electrode 80	549303	4060160	832
Electrode 160	549312	4060080	824
Electrode 240	549321	4060000	827
Electrode 320	549332	4059926	834
Electrode 400	549342	4059846	829
Electrode 480	549336	4059764	828
Electrode 560	549330	4059685	831
Electrode 640	549317	4059604	829
Electrode 720	549316	4059524	827
Electrode 800	549312	4059446	828
Electrode 880	549311	4059368	822
Electrode 960	549315	4059289	824
Electrode 1040	549315	4059208	822
Electrode 1120	549307	4059128	818
Electrode 1200	549300	4059051	818
Electrode 1280	549291	4058972	817
Electrode 1360	549261	4058896	819
Electrode 1440	549235	4058822	817
Electrode 1520	549210	4058749	813
Electrode 1600	549166	4058679	813
Electrode 1680	549120	4058614	812
Electrode 1760	549074	4058549	812
Electrode 1840	549031	4058478	807
Electrode 2000	548930	4058354	811
Electrode 2080	548875	4058295	811
Electrode 2160	548815	4058247	811
Electrode 2240	548756	4058191	810
Electrode 2320	548699	4058132	815
Electrode 2400	548641	4058079	812
Electrode 2480	548570	4058037	814
Electrode 2560	548501	4057997	814
Electrode 2640	548435	4057954	811
Electrode 2720	548379	4057898	807
Electrode 2800	548330	4057837	807
Electrode 2880	548275	4057779	805
Electrode 2960	548223	4057719	804

Appendix 1-6. Receiver station location of each CSAMT electrode for Line R.—Continued

[Coordinate system: Universal Transverse Mercator Zone 11, North American Datum of 1983; elevation is in meters above the North American Vertical Datum of 1988]

Electrode identifier	Easting (meters)	Northing (meters)	Elevation (meters)
Electrode 3040	548174	4057657	804
Electrode 3120	548107	4057614	802
Electrode 3200	548036	4057577	801
Electrode 3280	547970	4057534	798
Electrode 3360	547903	4057485	797
Electrode 3440	547848	4057429	798
Electrode 3520	547795	4057369	800
Electrode 3600	547728	4057321	800
Electrode 3760	547587	4057253	792
Electrode 3840	547518	4057216	794
Electrode 3920	547450	4057173	792
Electrode 4000	547396	4057114	791
Electrode 4080	547370	4057041	792
Electrode 4160	547352	4056966	792
Electrode 4240	547329	4056892	790
Electrode 4320	547301	4056817	789
Electrode 4400	547271	4056748	783
Electrode 4480	547229	4056678	782
Electrode 4560	547194	4056603	784
Electrode 4640	547154	4056536	788
Electrode 4720	547111	4056468	790
Electrode 4800	547067	4056401	790
Electrode 4880	547009	4056344	790
Electrode 4960	546947	4056293	784
Electrode 5040	546882	4056244	782
Electrode 5200	546745	4056167	786
Electrode 5280	546677	4056125	785
Electrode 5360	546606	4056083	788

Appendix 1-7. Receiver station location of each CSAMT electrode for Line T.

[Coordinate system: Universal Transverse Mercator Zone 11, North American Datum of 1983; elevation is in meters above the North American Vertical Datum of 1988]

Electrode identifier	Easting (meters)	Northing (meters)	Elevation (meters)
Electrode 0	550928	4059273	838
Electrode 80	550870	4059221	828
Electrode 160	550810	4059167	833
Electrode 320	550703	4059049	833
Electrode 400	550648	4058992	833
Electrode 480	550592	4058937	826
Electrode 560	550533	4058879	831
Electrode 640	550477	4058822	827
Electrode 720	550422	4058766	829
Electrode 800	550363	4058708	822
Electrode 880	550310	4058653	827
Electrode 960	550254	4058596	823
Electrode 1040	550200	4058543	821
Electrode 1120	550141	4058483	823
Electrode 1360	549973	4058314	815
Electrode 1440	549917	4058255	820
Electrode 1520	549861	4058198	822
Electrode 1600	549806	4058139	822
Electrode 1680	549753	4058085	823
Electrode 1760	549695	4058028	823
Electrode 1840	549638	4057972	820
Electrode 1920	549579	4057916	817
Electrode 2000	549524	4057859	813
Electrode 2080	549469	4057802	815
Electrode 2160	549411	4057745	812
Electrode 2240	549356	4057689	811
Electrode 2320	549299	4057634	810
Electrode 2400	549241	4057582	808
Electrode 2480	549184	4057526	812
Electrode 2560	549126	4057468	811
Electrode 2640	549070	4057412	809
Electrode 2720	549012	4057357	809
Electrode 2800	548954	4057297	811
Electrode 2880	548898	4057242	807
Electrode 2960	548842	4057186	808
Electrode 3440	548484	4056821	803
Electrode 3520	548426	4056766	799
Electrode 3600	548372	4056709	796

Appendix 1-7. Receiver station location of each CSAMT electrode for Line T.—Continued

[Coordinate system: Universal Transverse Mercator Zone 11, North American Datum of 1983; elevation is in meters above the North American Vertical Datum of 1988]

Electrode identifier	Easting (meters)	Northing (meters)	Elevation (meters)
Electrode 3680	548317	4056651	797
Electrode 3760	548258	4056595	794
Electrode 3840	548202	4056537	794
Electrode 3920	548145	4056481	792
Electrode 4000	548088	4056424	791
Electrode 4080	548031	4056369	791
Electrode 4160	547973	4056311	792
Electrode 4240	547917	4056254	790

Appendix 1-8. Receiver station location of each CSAMT electrode for Line W.

[Coordinate system: Universal Transverse Mercator Zone 11, North American Datum of 1983; elevation is in meters above the North American Vertical Datum of 1988]

Electrode identifier	Easting (meters)	Northing (meters)	Elevation (meters)
Electrode 400	550995	4057267	819
Electrode 480	550937	4057212	818
Electrode 560	550880	4057156	816
Electrode 640	550824	4057102	813
Electrode 720	550767	4057047	814
Electrode 800	550709	4056990	814
Electrode 880	550653	4056935	813
Electrode 960	550595	4056879	813
Electrode 1040	550537	4056824	812
Electrode 1120	550482	4056768	810
Electrode 1200	550424	4056713	811
Electrode 1600	550117	4056395	801
Electrode 1680	550062	4056338	801
Electrode 1760	550006	4056281	799
Electrode 1840	549950	4056223	798
Electrode 1920	549896	4056166	796
Electrode 2000	549840	4056108	796
Electrode 2080	549782	4056051	793
Electrode 2160	549726	4055994	795
Electrode 2240	549671	4055936	794
Electrode 2320	549615	4055880	793
Electrode 2400	549560	4055822	792
Electrode 2480	549503	4055766	792
Electrode 2560	549448	4055708	792
Electrode 2640	549392	4055652	792
Electrode 2720	549336	4055594	791
Electrode 2800	549280	4055538	789
Electrode 2880	549223	4055480	791
Electrode 2960	549168	4055424	794
Electrode 3040	549111	4055367	793
Electrode 3120	549055	4055310	792
Electrode 3200	548999	4055253	792

Produced in the Menlo Park Publishing Service Center, California
Manuscript approved for publication October 11, 2011

Macy and others—**Characterization of the Highway 95 Fault in Lower Fortymile Wash using Electrical and Electromagnetic Methods, Nye County, Nevada**–Scientific Investigations Report 2012–5060